IMPACT CHARACTERIZATION OF FRP PANELS AND T–PULL JOINT

By

GAJENDRA PANDEY

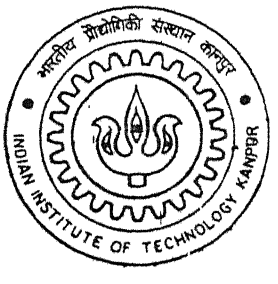

DEPARTMENT OF MECHANICAL ENGINEERING

Indian Institute of Technology Kanpur

FEBRUARY, 2002

IMPACT CHARACTERIZATION OF FRP PANELS AND T–PULL JOINT

A Thesis Submitted
in Partial Fulfillment of the Requirements
for the Degree of

MASTER OF TECHNOLOGY

By

GAJENDRA PANDEY

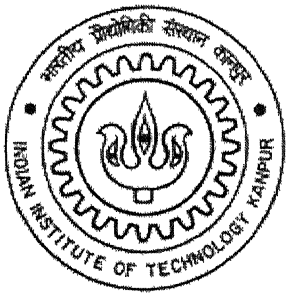

to the

Department of Mechanical Engineering

Indian Institute of Technology Kanpur

February, 2002

CERTIFICATE

It is certified that the work contained in this thesis entitled **"Impact Characterization of FRP Panels and T-Pull Joint"**, *by* **Gajendra Pandey**, *has been carried out under my supervision, and this work has not been submitted elsewhere for a degree.*

P Kumar

February, 2002

Dr. Prashant Kumar
Dept. of Mech. Engg.
Professor
I.I.T. Kanpur

dedicated to
MY PARENTS

Acknowledgement

I would like to express my deep sense of gratitude to my ever-cherished guide Dr. Prashant Kumar for his invaluable guidance and help throughout my M.Tech. Programme. I am sincerely thankful for his valuable suggestions in my academic as well as personal life.

I can not forget to thank Dr. V. Raghuram for his invaluable cooperation inspite of his busy schedule. He was always there with his helping hand whenever I felt the need of his expertise. His guidance was a big suppliment in making my work flawless.

Mr. Diwakar & Mr. Anurag deserve special thanks who were constantly involved with me throughout my thesis work and help me whole heartily. I would like to thanks Mr. B.D.Pandey, Mr. Pankaj and Mr. Ramchandra Tiwari for their kind cooperation throughout the work.

It gives me immense pleasure to recall my association with Dheeraj, Tinks, Ashish and Abhishek for their cooperation. I also wish to thank Ayush, Anup, Rahul, Kapil and all members of DESIGN group who made my stay at IITK, pleasant memory.

Finally I would like to express my gratitude to my parents and my dear brother who always encouraged and cooperated with me at all stages of my life.

Gajendra Pandey

ABSTRACT

Polymer composites are known for many attractive properties but their impact-induced resistance is poor. Impact of a foreign body affects the strength of composites considerably. Compression After Impact (CAI) properties becomes a critical parameter in design of structures especially in the aerospace applications. Thus one needs to perform impact tests on the polymer composite panels under controlled conditions and then determine compressive strength.

An air gun test setup is used to perform the impact tests under controlled conditions. An aluminium striker bar of mass 4.8 gm, length 15.5 mm and diameter 12.6 mm is used to impact the FRP panels of size 150 mm $\times$ 220 mm. The velocity of the striker bar is measured with the help of a laser beam intersecting the striker bar and recording the pulse on a digital oscilloscope. The velocity of the striker bar is controlled to have impact energy of 12 J.

Two types of specimens are used to determine the compressive strength after impact, (i) glassfiber angleply laminate (GAL) and (ii) glassfiber fabric laminate (GFL). After conducting experiments it is seen that the compressive strength of GAL specimens after impact is 15.7 MPa and that of the GFL specimen is 58.5 MPa. In comparison to GAL, the GFL specimens are thus found to possess considerably higher compressive strength after impact.

T-Joints are extensively used to make large FRP structures as one piece specially in aerospace industries. Impact of a foreign body affects the strength of T-Pull specimen considerably. A test facility to determine the tensile strength of T-Pull specimens after it is impacted by a striker bar is designed, fabricated and made functional. One test was performed on an unimpacted T-Pull specimen, supplied by NAL Bangalore, to establish that the setup works well.

Contents

List of Figures

List of Tables

Chapter 1

Introduction

1.1 Introduction

Todays scenario of technological development requires new materials capable of withstanding the service working and loading conditions, such as those experienced in the field of air and road transport, space ships, sports, etc. These requirements seek for materials which are lightweight, high strength, tough and resistant to corrosion. The demand for such materials with versatile properties encourages the search of new materials.

Polymer composites consists of two or more phases, each phase being chemically and physically different from the others. These materials have one or more discontinuous phases (fibres) embedded in continuous phase (matrix). The discontinuous phase is stronger and stiffer than continuous phase.

Polymer composites are known for their distinct properties such as high specific strength, fatigue and corrosion resistance, which depend on properties of constituents as well as on the behaviour of interface between the fibres and matrix. Though composites have positive feature of many attractive properties but they lack in impact induced resistance. Impact of a foreign body affects the different properties of a composite such as compressive strength, tensile strength, etc. To understand the effect of impact, tests are conducted under controlled conditions.

When a solid is subjected to any type of loading, static or impact, it

can absorb energy by two basic mechanisms: (1) creation of new surfaces and (2) material deformation. The material deformation occurs first. If the energy supplied is large enough, a crack may initiate and propagate, thus actuating the second energy-absorbing mechanism. The material deformation continues in advance of the crack during crack propagation.

The most of matrix materials (i.e. epoxy) used in composites are inherently brittle in nature. Moreover, in a laminate there is no reinforcement of fibres along the thickness; hence an interface is rich in matrix having low energy absorbing capacity at the interface. It makes them vulnerable to delamination failure under impact loading. The various factors that contribute to delamination of polymer composites are brittle nature of constituents, poor interface bonds, difference in properties of constituent elements like modulus, complex energy absorbing mechanisms, microcracks, and material discontinuities, etc. Due to low toughness of interface in polymer composite laminates, once a delaminates crack is initiated by an impact it propagates at very high speed. As a result even the impact of a small body impact (hailstorm, runway debris on airstrip, drop of work tool, etc.) causes extensive delamination around the point of impact. On the other hand, when a sheet of conventional metals is impacted by a foreign body usually it is not cracked because of local yielding. Further, the propagation of crack is inhibited owing to work hardening of metals. Therefore, impact loading causes more severe damage in composite materials as compared to conventional metals. The presence and growth of delamination crack results in the progressive reduction of stiffness and strength of composites.

In many engineering applications composite materials are subjected to high strain rate deformation or impact loads thus, it becomes important to know the impact behaviour of composites for both safe and efficient design.

A very common way to evaluate the impact properties of metals is to determine the toughness of materials by knowing the energy required to break a specimen of a particular geometry. The well known Charpy and Izod impact tests are very useful for metals for comparing the impact properties of different materials. For composites the fracture phenomenon is much more complex. The mode of fracture and therefore the absorbed energy during impact are influenced by various tests variables such as fibre orientation, specimen geometry, velocity of impact, etc. In fact, Charpy and Izod tests do not give the data of basic

physical significance. This has resulted in the development of the other type of testing setups i.e. Drop-Weight impact test, Air Gun impact test setup.

1.2 Literature Survey

The study of impact behavior of fibrous composite materials did not receive much attention until the mid-1960s. The early published results on the subject were obtained with a standard Charpy impact machine without any attempt to study the phenomenon of impact.

In 1970s L.J. Broutman and his associates performed extensive impact studies on specially built drop-weight impact-testing apparatus in which several experimental parameters could be easily varied. They performed their studies on glass-fiber-reinforced epoxy and polyester resin and on hybrid graphite-Kevlar-glass composites. Through high-speed photography, important observations on the phenomenon of fracture and associated energy-absorbing mechanisms were made. Experimental parameters, were varied, including fiber orientation, velocity of impact, drop weight and specimen dimensions.

Many works have been presented on damage due to impact on composite structures. Chaturvedi and Sierakowski (1983) observed that the interface of fibre composite laminates possess poor impact resistance. The interfaces were inherently weak due to saveral causes such as stress discontinuity at the interfaces, absence of high strength fibre reinforcement through the thickness, use of brittle matrix (e.g., epoxy) which bind the neighbouring plies. Joshi and Sun (1985) observed that one of the primary failure mechanisms of an angle play composite laminate when impacted by a foreign body is through the generation of transverse cracks within the rear ply by the flexural stresses. Malvern, Sierakowski and Takeda (1982) studied that the transverse cracks move inward until they reach an interface with another ply of different fibre orientation. The transverse cracks of high kinetic energy find it difficult to fracture fibre of next ply. Rather, they turn sideways to become interlaminar cracks due to inherent weak interfaces. Cantwell and Morton (1985) observed that the delamination also occurs on impact side of the laminate due to high contect stress.

Abbott, Jonas and Kassa poglou (1988) observed that the delamination

damage reduces the strength of laminate significantly. Saveral approaches are being tried to restrict the impact damage in a laminate. Gawahale (19990) reinforces interfaces with particles to restrict the impact impact damage in a laminate. Liu (1990) observed that the damage due to impact also restrict by stitching the plies together. Meester, Verposest and Wevers introduces stitching of plies together but by using 3-dimensional weaver. Sun and Rechak (1998) found that the damage due to imapct in a laminate is restricted by toughening the matrix.

It had also been realize that both the free surfaces of the laminate also affect the delamination damage. Gillespie, Maikuma and Whitnet (1989) observed that the delamination at the rear most interface, which are caused by the transverse cracks in the rear ply under flexural stresses, propagate to interior interfaces. Clark (1989) found that on the impact side of the laminate, dalamination occurs due to high contect stresses. The delamination damage also propagate to interior plies with the help of transverse cracks in the intermediate plies. Therefore, if the generation of transverse cracks in the surface plies can be controlled, it may possible to restrict the impact damage on interior interfaces.

Stellbrink (1983) improved the impact strength of CFRP by covering its laminate with a thin E-glass fabric. Kumar and Rai (1990) studed the impact induced damage on an angleply KFRP laminate the surface of which was replaced by a balanced ply of glass fabric. The laminates were impacted by a stainless steel projectile accelerated through an air gun. They found that the replacement of surface plies reduced the projected impact damage for incident impact energies greater than 6.5 J per mm thickness of the laminates. Zhou (1998) showed that it is essential to have an impact rig designed with certain traits along with other selected impact conditions so that dominant damage mechanisms occurring during impact can be identified with the threshold forces of recorded impact force-time curves. Impact force data are then used to study impact damage resistance. Olsson (1999) showed that the response type is governed by the impactor plate mass ratio and derived a criterion for small-mass (wave controlled) impact response of orthotropic plates. Lee, Cheon and Im (1999) studed the impact behaviour of sheet moulding compounds (SMC) by setting up a drop weight impact test system. Using this system, the dissipated impact energies of SMC flat plates were measured to investigate the influence of the mass and shape of impactor, initial velocity, and specimen thickness on the impact behaviour.

Lou, Green and Morrison (2001) investigate the impact damage initiation and propagation in composite plates. The main characters of impact damage can be predicted by introducing both threshold strength and propagation strength for matrix cracking. The threshold strength controls whether the damage occurs in the composite structures, whereas the propagation strength determines the extent to which the damage develops. Hou, petrinic and Ruiz (2001) showed an improved delamination criterion for laminated composites structures. Out-of-plane stresses have been taken into consideration for damage initiation. Remmers and Borst (2001) showed some experimental observations regarding delamination buckling in Glare and on the basis of these observations, a numerical model was constructed as a meso-mechanical level. In this approach, solid-like shell elements were used to model the individual layers. They were connected by interface elements, which are capable of modeling delamination between the layers. Naik and Meduri (2001) studed the effect of laminate configuration on the impact behaviour of different polymer-matrix composites subjected to a transverse central low-velocity point impact load. For this a 3D transient finite-element analysis code using a modified Hertz law has been used.

Many investigators have been reported on the compressive strength of the composite structures. Curtis, Hawyes and Souts (2000) predicts the compressive strength of composite laminates containing an open-hole by fracture mechanics based models such as linear softening cohesive zone model. In this approach they replaced the inelastic deformation associated with an equivalent crack loaded on its faces by a bridging traction which was linearly reduced with the crack closing displacement. Asp, Nilsson and Singh (2000) focuses on compression tests of carbon fibre/epoxy panels with embedded artificial delaminations at various depths. Accompanying tests on undamaged and impact-damage panels were reported and the relevance of the tests on artificially delaminated panels was assessed. In the experiments both the artificially delaminated and the impacted plates failed by delamination growth. Herszberg, Leong and Khondker (2001) showed the effect of biaxially deforming weft Milano rib fabric on the overall composite compressive properties for a glass/vinyl-ester knittes composite. They found that the compressive properties of these structures, on the whole, appeared to be closer to isotropic and relatively intensive to fibre deformation. Short, Guild and Pavier (2001) studed the effect of delamination geometry on the compressive behaviour of laminated composite materials. They carried out compression tests on GFRP specimens containing

artificial delamination of various geometry, created by inserting PTFE film into the laminate during layup.

Besant, Davies and Hitchings (2001) presents a finite element procedure for predicting the impact behaviour under low velocity impact of sandwich panels consisting of brittle composite skins supported by a ductile core. Sandwich panels with carbon fibre skins and aluminium cores are used. This study showed that honeycomb is a good absorber of impact energy. Johnson, Pickett and Rozycki (2001) describes materials modeling and numerical simulation of impact response of fibre-reinforced composite structures. A continuum damage-mechanics (CMD) model for fibre-reinforced composites is developed as a framework within which both in-ply and delamination failure may be modeled during impact loading.

1.3 Problem Definition

Two problems are studed (i) compressive strength of a panel after it is impacted with a foreign body and (ii) tensile strength of a T-joint after it is impacted. Chapter 2 describes the experimental setup for impact test and compression test for FRP panels under controlled conditions of buckling guides to suppress the buckling of panels. Chapter 3 discusses the impact and pulling setup of T-specimen. In chapter 4 the results of experiments of compression after test presented. Chapter 5 presents the conclusions of the works and suggestions for future work.

Chapter 2

Experimental Technique

2.1 Introduction

Impact induced damage in composite structures is perhaps one of the most important consideration that inhibits widespread application of composite materials. A sufficient intensity of such a loading causes damage which affects not only structural response during loading but also reduces structural strength capacity in subsequent static loading.

In this chapter, procedures for experimental technique are discussed to determine the compressive strength of FRP composites subjected to impacted load with low velocity. In order to produce damage in a specimen a short projectile accelerated by an air gun is used. The specimen is then compressed in the Material Test System.

2.2 Impact Setup

The schematic diagram of the impact setup is shown in Fig 2.1. Nitrogen gas is filled from a gas cylinder (1) in the gas chamber (5) and the pressure in the gas chamber is monitored by the pressure gauge (3) and controlled by the release valve (4). The pressure gauge and the release valve are mounted

on the Manifold (2) which connects the air gas cylinder and the gas chamber. In order to accelerate the projectile in the gun barrel (7), gas in the gas chamber is released through the solenoid valve (6). Laser torch held by a laser torch holding stand (10) for measurement of velocity of projectile is fastened at the mouth of the gun barrel. The gun barrel is supported by gun barrel stand (8, 9). The projectile impacts the specimen which is clamped in the specimen mount (11). The whole setup is supported by a frame (12).

2.2.1 Specimen

In the present work, study is mainly focussed on glassfibre fabric/epoxy laminates with following configuration:

- $[0/45/-45/90/90/-45/45/0]_{2s}$, glass fabric reinforced epoxy (Quasi-isotropic Laminate), Glassfiber Angleply Laminate (GAL)
- $[0]_{24}$, glass fabric reinforced epoxy, Glassfiber Fabric Laminate (GFL).

The following section will disscuss about specimen geometry, raw materials used, preparation of preforms, their cross section, laminate preparation from the preforms and specimen preparation from laminates.

Specimen Dimensions

The dimensions of the specimen panel (Fig. 2.2) are:

Length	220 mm
Width	150 mm
Thickness	2.0 - 4.0 mm

Specimen Preparation

Glassfiber fabric as reinforcement and epoxy resin mixture as matrix are the two basic materials used for the preparation of specimen.

The glassfiber fabric used are purchased from Harshdeep Industries, Ahemdabad. Its specifications are as follows:

Number of yarns per 25 mm in warp = 40
Number of yarns per 25 mm in weft = 36
Area Density =146 gm/cm^2
Width of fabric =150 mm.

Specimen preparation starts by employing prepeg tapes, which are prepared on Prepreg Machine, developed by Kumar et al. (1995). The matrix consists of epoxy LY-556 and hardener HT976 (4,4 - Diaminodiphenyl Sulphone) along with accelerator XY73 (used for proper cutting of epoxy) and silane (used for good wetting of fibers) in the weight ratio of 100:35:1.5:0.5. The silane, epoxy and accelerator are purchased from Ciba-Geigy Ltd. Bombay and hardener is purchased from Advanced Formulated Compounds, Atlanta U.S.A. The prepregs are made at 95^{o}C and stored at -18^{o}C.

The prepregs are cut to an approximate length of 250 mm and the layers of the prepregs are stacked on a Glass Fiber reinforced Teflon sheet (GFT sheet). Usually 8 layers of prepreg tapes gives 1 mm thickness to the GFL specimen and 1.5 mm thickness to the GAL specimen. In the present work, 24 layers of prepregs are used for GFL specimen and 16 layers are used for GAL specimen. For GFL specimen another GFT sheet is placed over the stack of the prepregs (Fig. 2.3). In order to facilitate the flowing out of extra epoxy and air bubbles during the curing of preform, the GFT sheets are perforated with holes of approximately 1 mm diameter and at approximately 10 mm apart in both directions. Then it is placed between two breather sheets which are made of woolen blanket of area density 360 gm/m^2 approximately. This woolen blanket is purchased locally. The entire set is sandwitched between another set of GFT sheets with no holes. These sheets protect platens of press from epoxy coming out while curing. For GAL specimen the stack is placed between two GFT sheets with no holes and a strip of 40 mm width (approximately) of woolen blanket is placed around it to facilitate the flowing out of extra epoxy. The sandwich is then placed in between the platens of a hydraulic press to prepare the laminate.

The fixture used for laminate preparation is shown in Fig. 2.3. The platens of hydraulic press is used to apply pressure and temperature. The curing

cycle is completed in three stages. First of all, temperature is increased to 120°C and maintained for one hour. During this phase pressure is not applied. In the second phase, pressure is applied and gradually increased to 7 bar and the specimen is kept at this condition upto one hour. At this stage the temperature is maintained at 120°C. For postcuring, the same pressure is maintained and the temperature is increased to 150°C and kept for next hour. Then the laminate is allowed to cool down slowly to room temperature, which takes about 24 hours. Then the laminate is taken out from the press and is trimmed by a diamond cutter to achieve proper dimensions.

2.2.2 Breach Assembly of Air Gun

The air gas chamber is made of stainless steel and stores the compressed Nitrogen gas at a predetermined pressure. It is attached to the air gun barrel by a solenoid valve. The nitrogen gas in the gas chamber is fed from a gas cylinder filled with nitrogen. The barrel used was made in the Field Gun Factory Kanpur and its specifications are:

Bore Diameter	12.65 mm
Outer Diameter	25 mm
Length	1000 mm

A manifold is attached to the gas chamber on which a pressure gauge is mounted to measure the gas pressure accurately. A release valve is attached to the manifold to remove the extra gas from the gas chamber.

The solenoid valve is one of the important part of the setup. It is an electromechanical device that utilizes a solenoid coil to control the opening and closing of the valve orifice. Valve position is directly proportional to the applied current. The specifications of the solenoid valve used are:

Type	IMVD–10
Volts	230 volts
C/S	50
Watt	8

Max. temp.	100°C
Max. pressure.	14—17 atmosphere
Orifice size	10 mm

A cylindrical projectile of aluminium is used to strike the specimen. The dimensions of projectile is shown in Fig. 2.4.

2.2.3 Base Channel

The bottom mild steel channel is used to mount the whole setup. The dimensions of the channel are as follows:

Width	200 mm
Height	75 mm
Length	5 m

The gun barrel is supported on two stands which are fastened to the bottom channel. In order to facilitate the recoil mobility of gas chamber (back and forth), it is guided on both sides by angles. The angles are bolted on the bottom channel.

2.2.4 Mounting of Specimen

The specimen mounting arrangement constitutes three parts, rear base frame, rear mount plate, and front mount plate. Assembly of mounting arrangement is shown in Fig. 2.5.

The rear mount plate, as shown in Fig. 2.6(a), is made of rigid mild steel plate of thickness 22–mm. A wide groove of 1.7–mm depth and 150.3–mm wide is cut in the plate so that specimen could be slided into the groove. A 125–mm square hole is cut in the rear mount plate. A rectangular frame shown in Fig. 2.6(b), of 200–mm×175–mm external dimensions and 125–mm square hole is used to clamp the specimen on the rear mount plate with the help of eight M10 capscrews as shown in Fig. 2.7. Both the rear and the front mount plates have the sufficient thickness to resist any deformation while testing. The surfaces

of the plates, which are in contact with the specimen, are machined properly to avoid specimen surfaces being scratched.

The rear mount is fastened to the rear base frame with four M10 screws. The rear base frame made of 10 mm thick web is sufficiently stiff and strong. The specimen mount assembly is fastened on the bottom base channel as shown in Fig. 2.7.

2.2.5 Velocity Measurement Device

In this section, the measurement system to determine velocity of projectile after it comes out of the barrel of the air gun, is discussed. The concept used for velocity measurement is, " the velocity of a body of length L crossing any point A in time t is L/t ".

The velocity measurement device is mounted at a small distance (few mm) away from the mouth of the gun barrel. A laser torch is used to generate a laser beam which strikes the photodiode on the other side of the barrel as shown in the Fig. 2.8. The photodiode is connected to the oscilloscope through a circuit which will be discussed in subsequent section. The laser torch and the photodiode is centrally aligned with the gun barrel. When laser beam strikes the photodiode, a line voltage of 5 volts is developed in the circuit and displayed on the screen of the oscilloscope. As the projectile cuts the laser beam, resistance of the photodiode suddenly increases and circuit voltage drops to zero. Thus the oscilloscope shows a pulse as shown in the Fig. 2.9. The time of travel (t) of the projectile can be computed from this pulse. If the length of the projectile is L, the velocity is L/t.

Circuit Diagram

The circuit connecting oscilloscope with photodiode is shown in Fig. 2.10. The photodiode is connected in reverse biased mode with a power supply of 5 volts. In the reverse biased mode, initially the photodiode has a very high resistance and no current flows through the circuit. As the laser beam

falls on the diode, a conduction path is generated which decreases the resistance close to zero and current starts to flow. A voltage equals to the voltage of power supply comes across the point A and B as shown in the Fig. 2.10. Thus, the initial setting corresponds to the laser light falling in the photodiode with 5 volt input to the oscilloscope. As the front end of the projectile cuts the laser beam the voltage drops to zero but it is recovered again when the rear end of the projectile passes the laser beam. Thus the rise and fall times of the pulse are obtained. However, initiation of rise and fall are taken as the representative values and they can be read with an accuracy of ± 0.5 μs.

Laser Torch and Photodiode Holding Devices

The holding devices used in this setup can move the laser torch in both X (horizontal) and Y (vertical) direction. An X-Y vernier alignment also employed to hold the laser torch so as to align the laser light to pass through the centre of the barrel. The holding arrangement of laser torch is mounted vertically on the bottom channel of the air gun setup. The laser torch is clamped to a holding block and the holding block is bolted in the X-Y alignment system.

The holding arrangement for photodiode can move in X and Y direction and can rotate so as to align the photodiode along the laser beam. The mounting stand for photodiode is shown in Fig. 2.11. Photodiode is embedded in a thermocol block mounted on the plate A with the help of the screw B. The plate A, integrated with the rod C, is mounted on rod F (integrated with base plate) through a slide D. Screw B allows the diode to move in the direction parallel to the axis of the barrel over plate A. Block D allows the vertical motion and rotation as well with the help of screw E. This arrangement facilitates all required motions to the photodiode.

Measurement of Velocity and Energy of Projectile

The velocity of projectile is measured by transfering the data to a personal computer through GPIB software. The data is then plotted with the help of GNUPLOT software. One can magnify the plot to measure the time

of flight of projectile upto the accuracy of ± 0.5 μs. To find the velocity and energy of impact of projectile, all the three quantities like length, time and mass are measured accurately.

2.3 Compression After Impact Test

Static uniaxial compression test is done to measure the residual compressive strength of a FRP panel after the impact. The procedure for impact test is discussed in previous sections. In this and the subsequent sections, procedure for estimating the compressive strength of damaged panels will be discussed.

The Compression test is done in a controlled environment, to prevent buckling of the panel during compression. Material Test System—Model 810 (10 ton capacity) is used for compression test. Machine uses the hydraulic power supply, which provides hydraulic fluid under pressure upto 21 MPa, to servovalves for actuator operation. Machine has Hydraulic Wedge Grip (model number 647) to clamp the specimen for testing purpose and a microconsole (model number 458.20) for its electronic control.

2.3.1 Specimen Preparation

Before loading the specimen in the compression test setup, the impacted panel needs some preparation. This section deals with the specimen geometry and its preparation after impact. The dimensions of specimen used in compression test are shown in Fig. 2.12. The impacted specimen is reduced to 100 mm width by cutting the edges. On this specimen, tabs of length 60 mm are bonded on each end and on both sides. The tabs are made of glass fabric reinforced polymer composite and are of 2 mm thickness. The preparation procedure and raw materials of tabs are same as that of the specimen as discussed in Section 2.2. To prepare the tab panel 16 plies of glass fabric prepreg are used.

2.3.2 Specimen Marking

Before compression, the specimen should be properly aligned with machine in following procedure to avoid buckling during compression.

The rectangles $ABCD$ and $A'B'C'D'$ are marked on the tabs, as shown in Fig. 2.13, for proper alignment of specimen in the grip of the machine whereas rectangle $EFGH$ is marked to assure the proper setting of buckling guides (discussed subsequently). The strain gauges are attached on both the faces at point I marked on the specimen as shown in Fig. 2.13. This point is at distance of 25 mm from both the tab ends as well as from the side of the specimen. "Araldite" is used as bonding agent for bonding of strain gauges. Strain gauges are imported from Tokyo Sokki Kenkyujo Co. Ltd., Tokyo, Japan, and specially designed to be used for composites. The specifications of strain gauge are:

Type	Electrical Foil Type
Resistance	120±0.2 Ω
Gauge Length	2 mm
Gauge Factor	2.11

In order to avoid buckling, buckling guide of mild steel is used. The buckling guide consists of two plates Front Buckling Guide and Rear Buckling Guide, shown in Fig. 2.14(a) and 2.14(b). The guides are sufficiently strong to resist any deformation in the present loading condition. The guides are clamped around the specimen with the help of four M12 bolts. The assembly of specimen with buckling guides is shown in Fig. 2.15 and a photograph showing the specimen holds between the jaws of MTS is shown in Fig. 2.16. Two rubber pads are inserted between the buckling guides; these rubber pads work like springs. During tightening of bolts of the Buckling Guides, distance between them is adjusted such that it is marginally higher than the specimen thickness (within 0.05 mm) with the help of a feeler gauge.

The buckling guide assembly is heavy because they are made of thick mild steel plates. In order that the weight of the buckling guide is not supported

by the specimen, two chamfered holes are made in line in both the buckling guides, and the whole assembly is suspended from the top frame of the MTS machine with the help of two strong and flexible strings.

Two types of data are recorded during the test, applied load and strains in the direction of load. The applied load is measured with the help of a load cell that is provided with the MTS. The strain gauge in the direction of loading is measured by using strain gauges. Load cell and strain gauges are connected to the Virtual Instrumentation (VI) to monitor them continuously during the test. Details of VI are discussed in the subsequent sections.

2.3.3 Virtual Instrumentation

In the compression test, Virtual Instrument is used for measuring the strain and load on the specimen. The block diagram of VI connecting MTS and computer is shown in Fig. 2.17. The signals from strain gauges are fed to a strain gauge signal condition card (model SC 2403–SG, National Instruments, USA). The strain gauge signal condition card is configured for recording signals in quarter bridge mode. The signals are then fed to an analog to digital card (model PCI 6024E, National Instruments, USA) for conversion of analog signal to digital signals. A virtual instrument is developed using LABVIEW program for recording strain signals from strain gauge and load signals from load cell.

2.4 Experimental Procedure

In this study, a projectile with comparatively lesser mass is deliberately chosen, since in the present work the study is intended to the after effect of low energy and high velocity impact. The laminate is rigidly fixed to the mountings as described in Section 2.2.4. The projectile is accelerated in Gun Barrel through gas pressure. The Nitrogen gas filled in the gas chamber is released through solenoid valve to accelerate the projectile . Pressure gauge and release valve are mounted on the manifold which in turn mounted between the gas cylinder and gas chamber. The velocity of the projectile is controlled by controlling the gas

pressure. With the help of pressure gauge, one can know the gas pressure inside the gas chamber, extra gas can be released with the help of release valve. The specimen mount is positioned such that the projectile hits the specimen at its centre.

The impacted specimen is then prepared for compression test as discussed in section 2.3. After holding the specimen between buckling guides, it is mounted on MTS using the wedge section friction grips of machine, upto the depth of 30 mm from both ends. The proper alignment of the specimen in the jaws is assured; the proper spacing between buckling guide plates and specimen is set within 0.05 mm using feeler gauges. Buckling guides are suspended symmetrically from the top frame on the MTS as described previously in this Chapter. The strain gauges and load cell are then connected to the VI as described earlier. After mounting specimen on to MTS, it is loaded monotonically upto the failure at a rate of 4.0 mm/min. The data (load and strain) are continuously recorded in the computer during the test through VI. Stress v/s strain curves are plotted using these data.

2.5 Closure

The work presented in this chapter describes the Impact test setup and compression setup, together with the experimental procedure. Successful tests are carried on FRP panels with the help of the described setup.

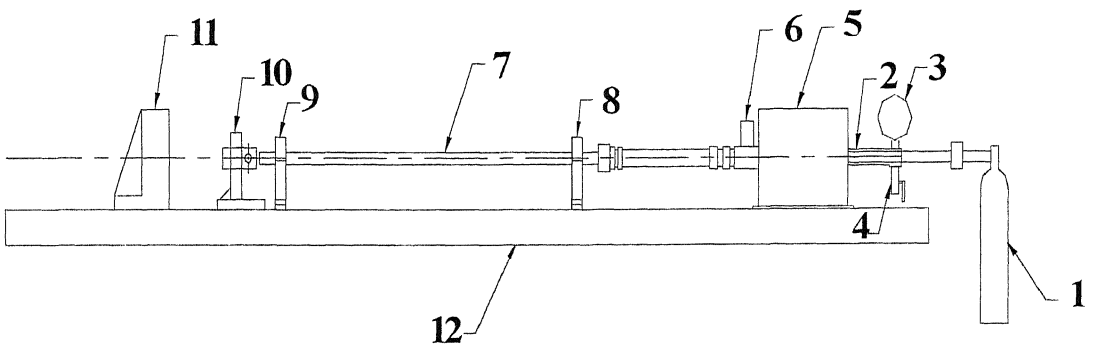

1. Air Gas Cylinder
2. Manifold
3. Pressure Gauge
4. Release Valve
5. Gas Chamber
6. Solenoid Valve
7. Gun Barrel
8. Stand to hold Gun Barrel
9. Stand to hold Gun Barrel
10. Laser Torch holding stand
11. Specimen Mount
12. Frame

Fig 2.1 Schematic diagram of Impact Test Setup

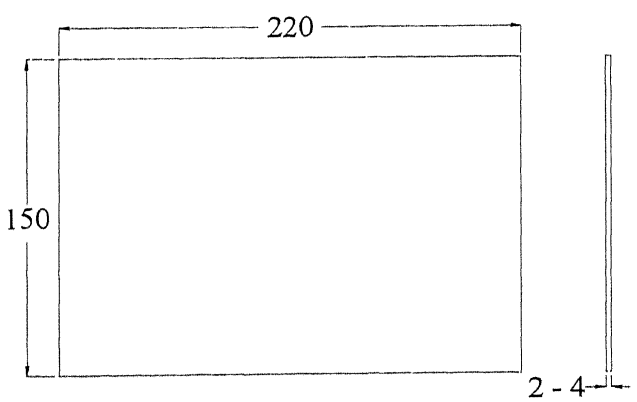

Fig. 2.2 Dimensions of Specimen used

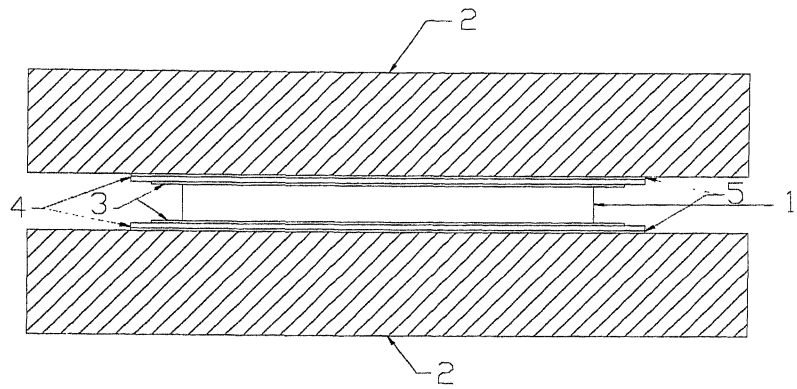

1. Laminate
2. Heated Platens of Press
3. GFT sheets with perforated holes
4. Breathers
5. GFT sheets

Fig. 2.3 Curing of laminate in a hydraulic press

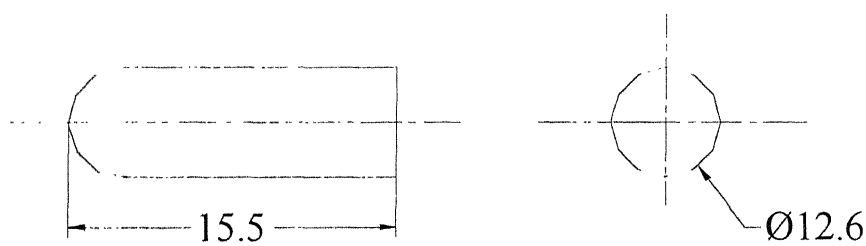

Fig. 2.4 Dimensions of projectile used

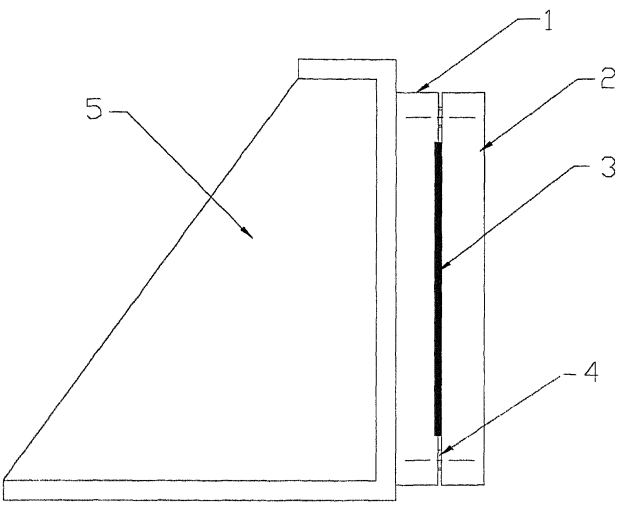

1. Rear mount plate
2. Front mount plate
3. Specimen
4. Bolts
5. Rear base frame

Fig. 2.5 Schematic View of mounting arrangement of Specimen

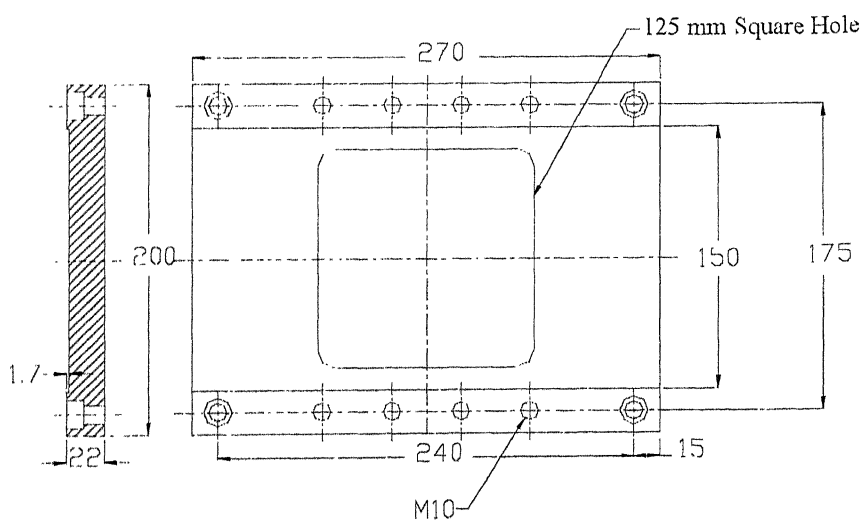

Fig. 2.6(a) Rear mount plate with shallow groove and centered hole

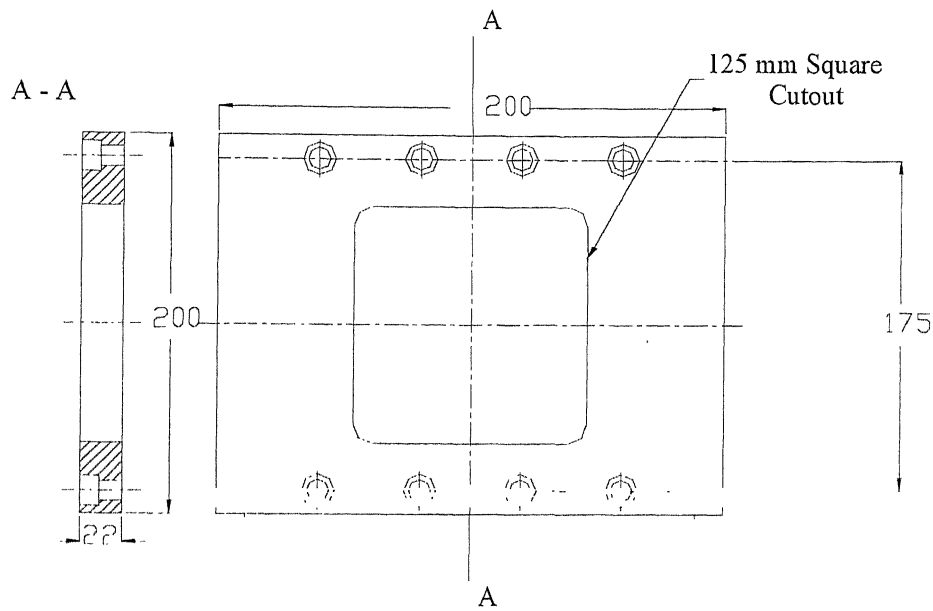

Fig. 2.6(b) Front mount Plate

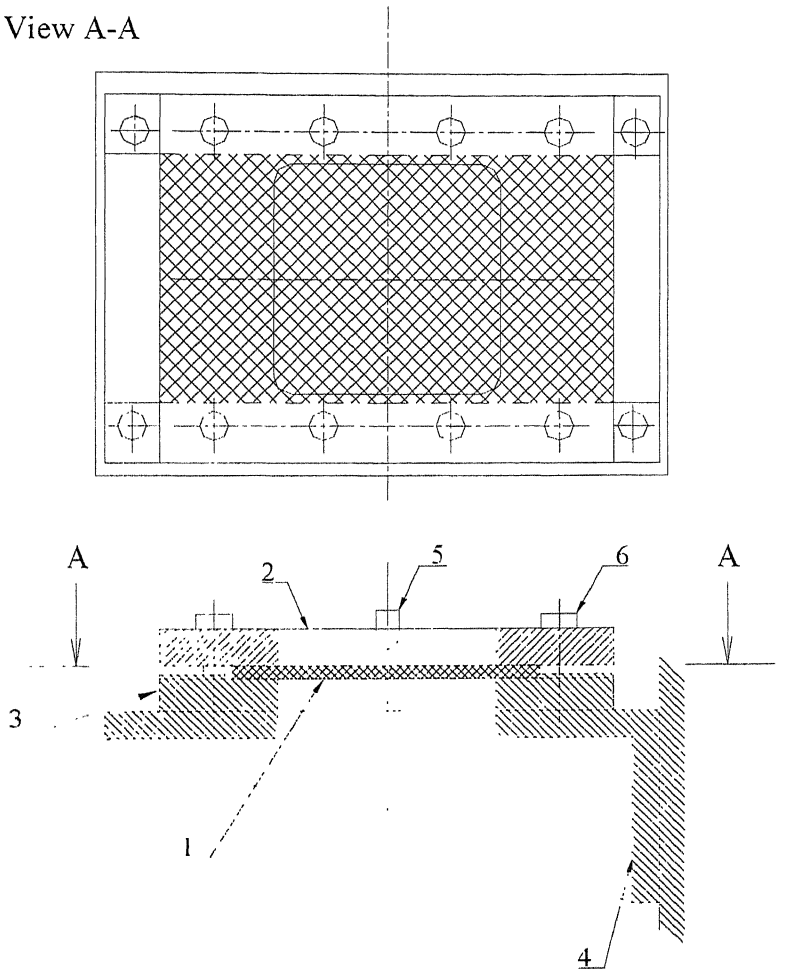

1. Specimen
2. Front pressing frame
3. Specimen support plate
4. Mounting frame
5. Projectile
6. Clamping cap screw

Fig. 2.7 Schematic diagram of fixture to mount the specimen

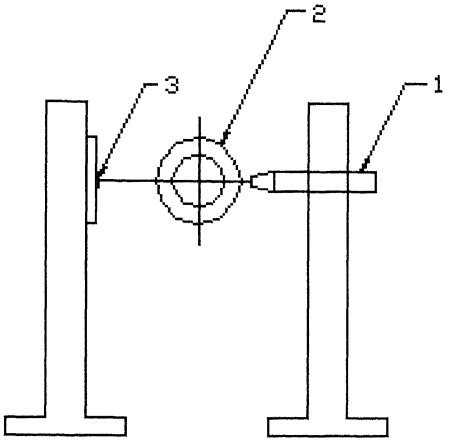

1. Laser Torch
2. Gun barrel
3. Photodiode

Fig. 2.8 Schematic View of Velocity measurement device

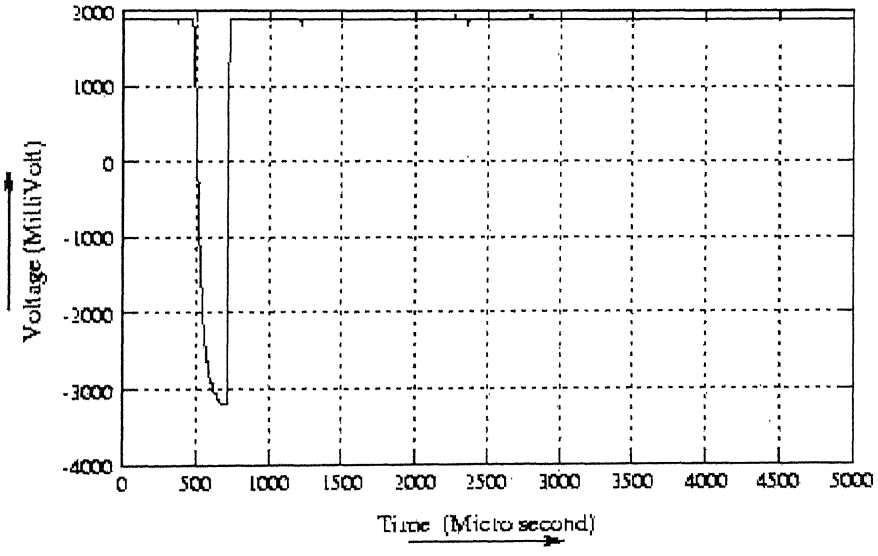

Fig. 2.9 Voltage Pulse displayed by Digital Oscilloscope for measurement of Velocity

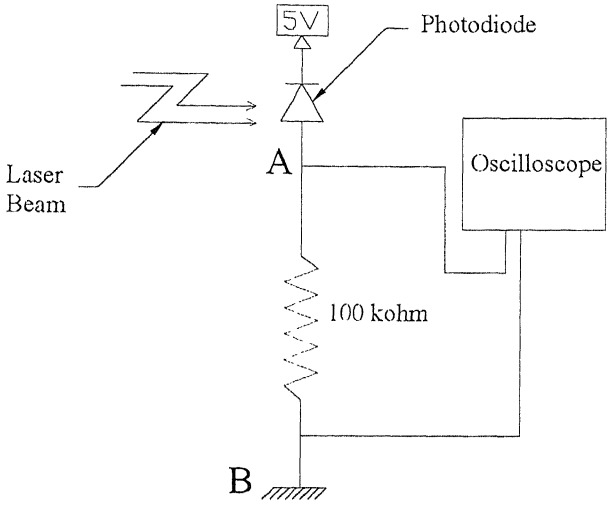

Fig. 2.10 Circuit diagram for Velocity Measurement

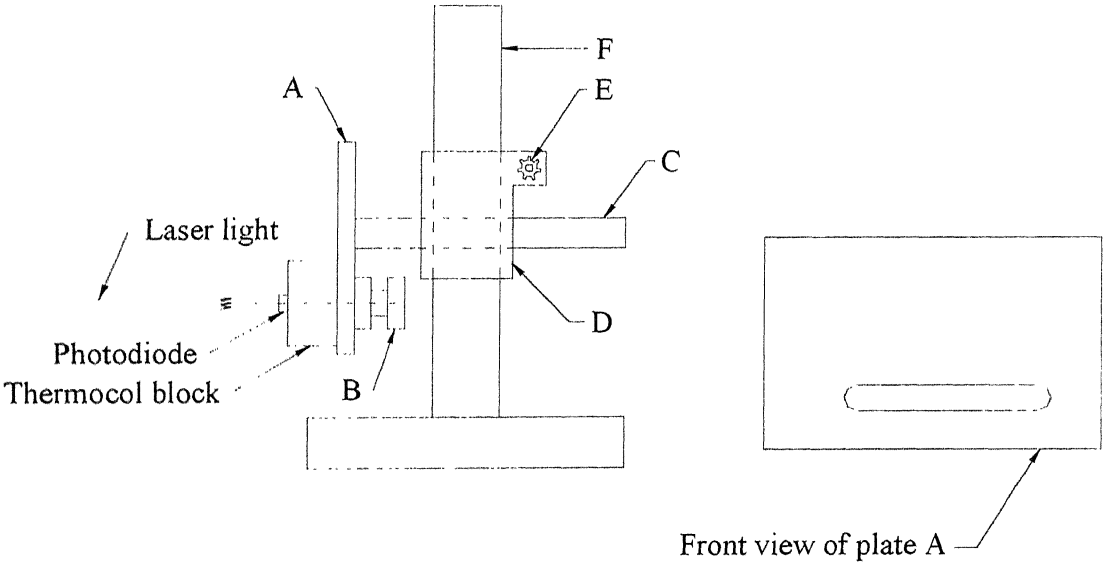

Fig. 2.11 Mounting stand for Photodiode

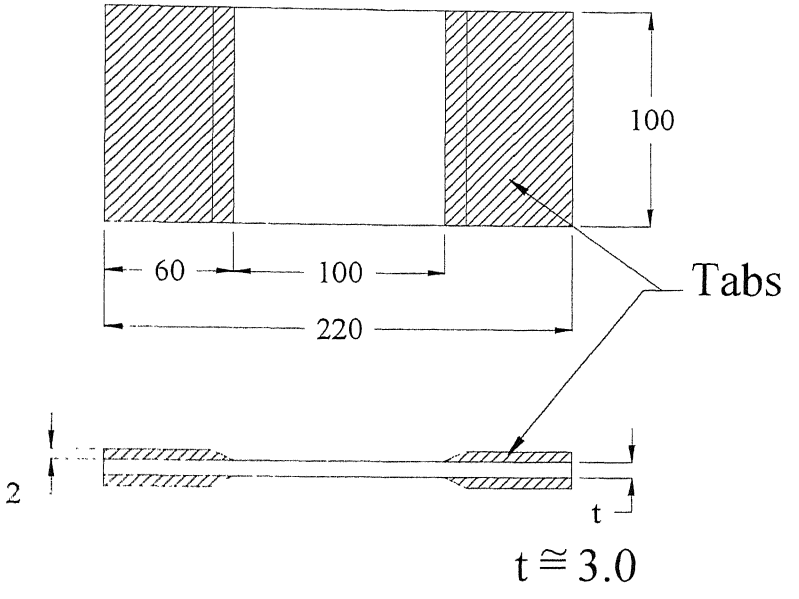

Fig. 2.12 Dimensions of specimen used for compression after impact test

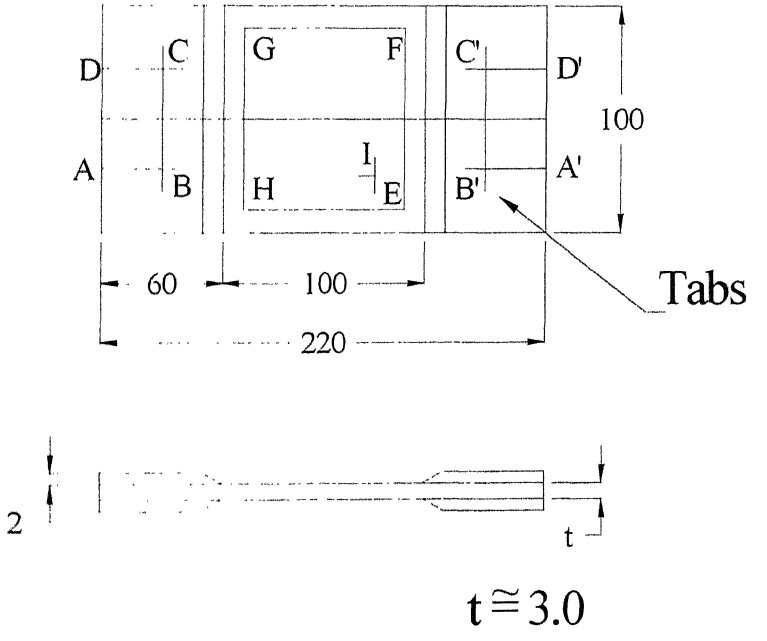

Fig. 2.13 Marked specimen before compression test

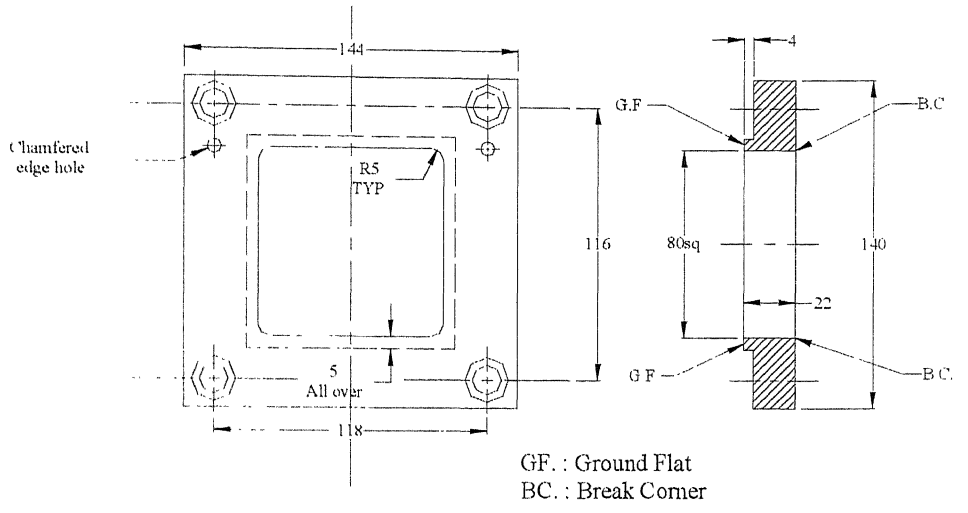

Fig. 2.14(a) Front Buckling guide plate

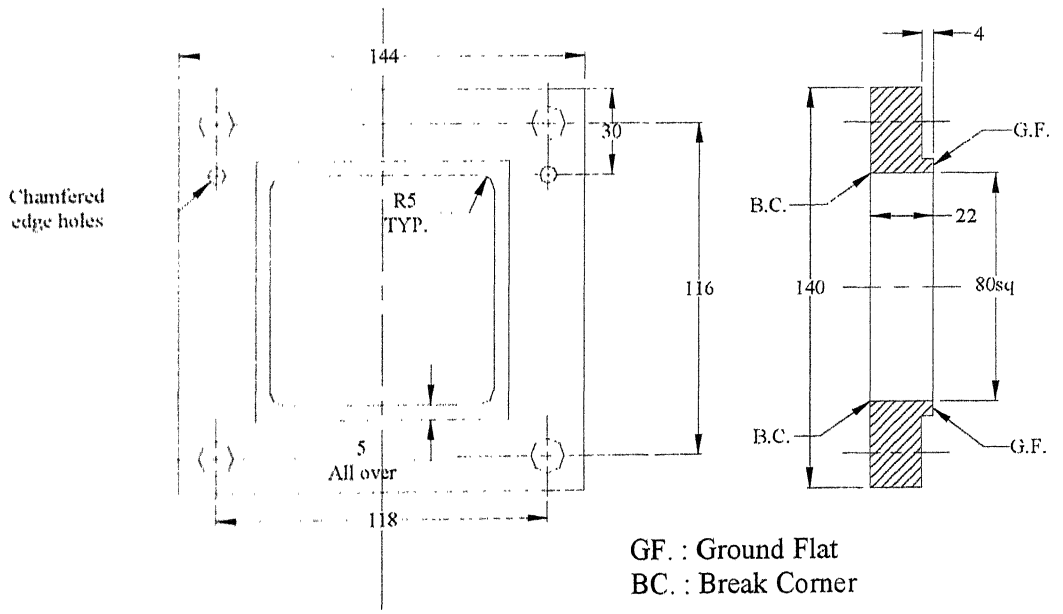

Fig. 2.14(b) Rear Buckling guide plate

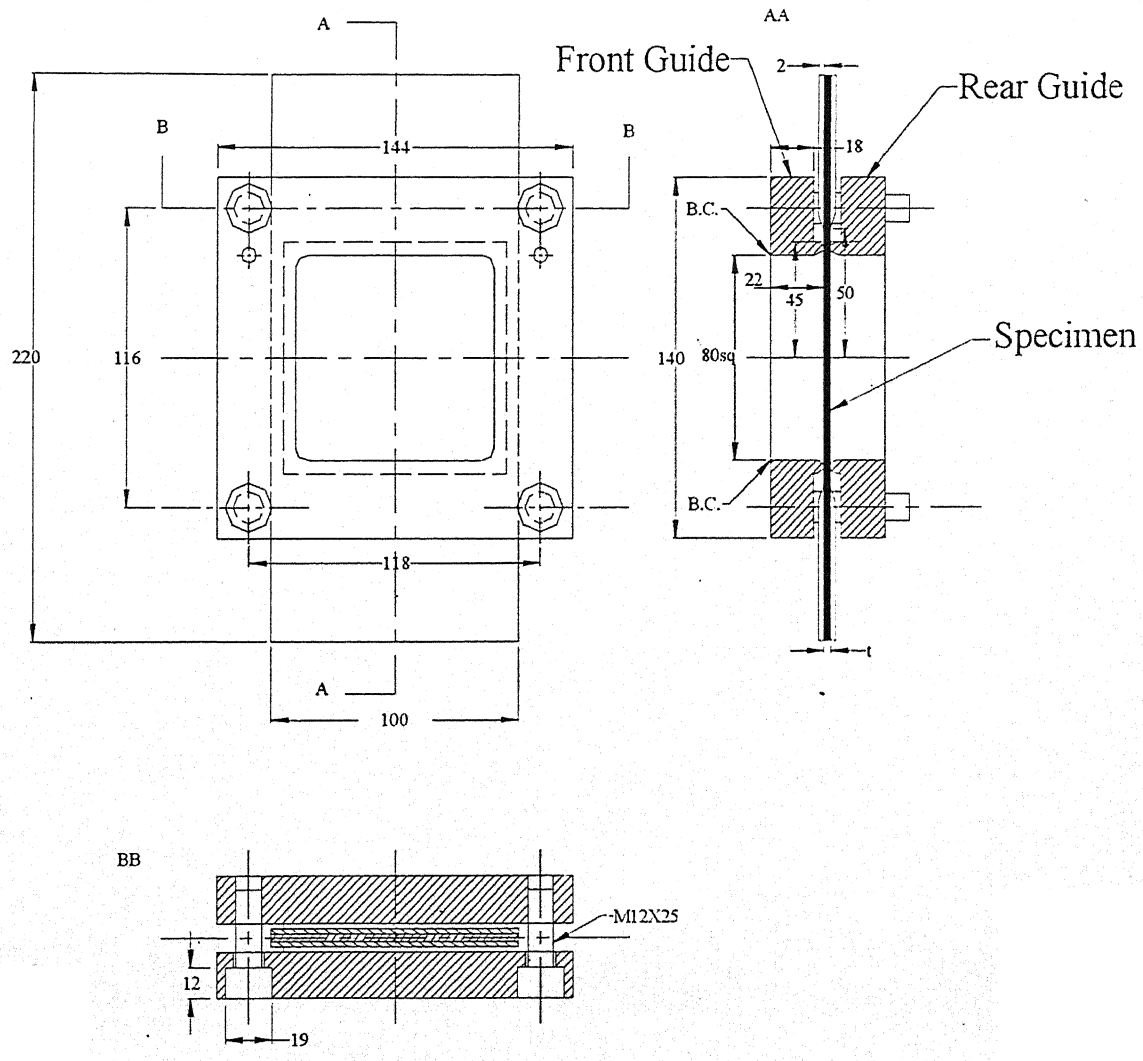

Fig. 2.15 Assembly of specimen with buckling guides

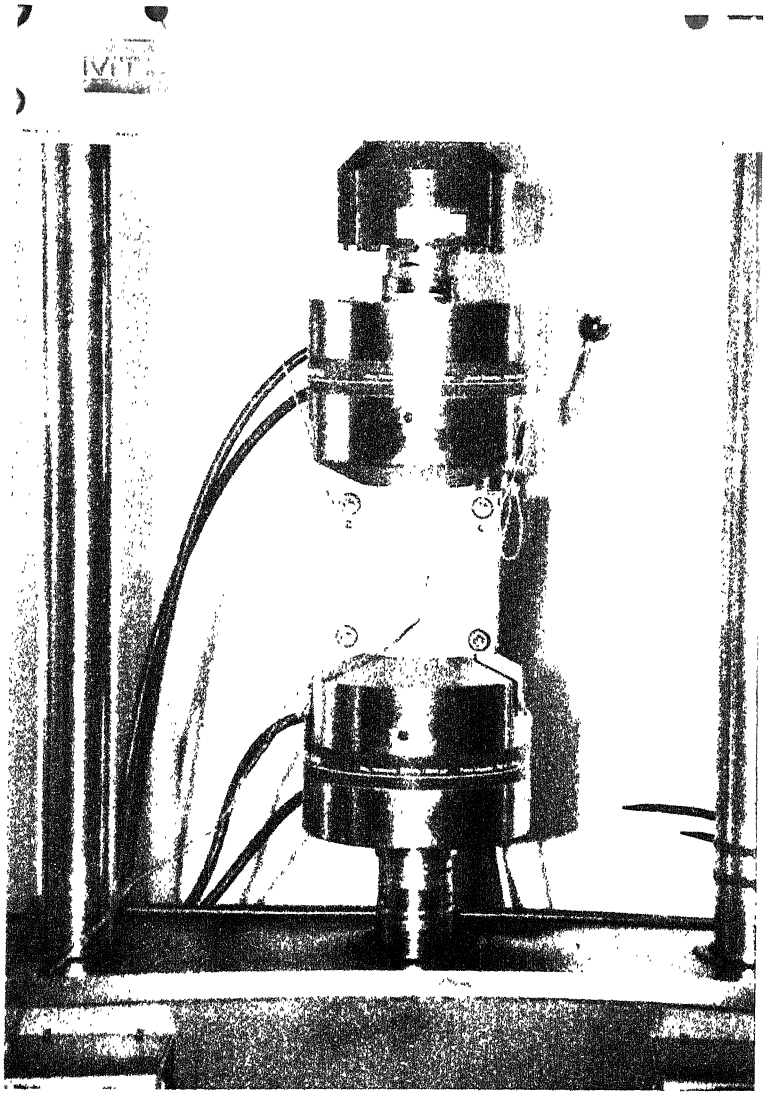

Fig. 2.16 Photograph showing the specimen holds between the jaws of MTS

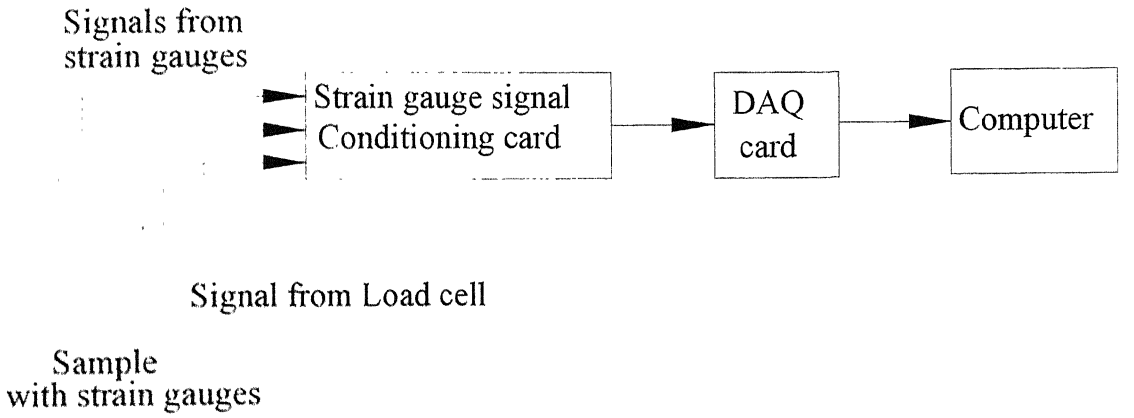

Fig. 2.17 Block diagram of Virtual Instrumentation setup using a D/A card

Chapter 3

Characterization of T–Pull Specimen

3.1 Introduction

Aeronautical Development Agency (ADA) is in process of developing a wing of Light Combat Aircraft (LCA) such that the entire wing is made of a single component (one piece structure) of CFRP. In the proposed wing, many T-joints are used to connect the panels to make a one piece structure of aircraft wing. It is therefore important to characterize a T-joints. The present chapter deals with the design and fabrication of a test setup to determine pulling strength of a T-joint after it is impacted in a controlled manner. Several organizations, NAL Bangalore, IISc Bangalore and IIT Kanpur are involved in the study of T specimen.

3.2 Specimen Definition

The T-specimens are supplied by NAL Bangalore. They are made of CFRP and have varying flange thickness (Fig. 3.1). The flange thickness (t_1)varies from 2.4 mm to 6mm. The flange width of a specimen, as shown in Fig. 3.1, is 80 mm, plydrop length (p) varies from 94 mm to 99 mm and total length of flange (l) varies from 170 mm to 179 mm. Web thickness (t_2) of the

T-joint varies from 2.9 mm to 3.1 mm and its web height (h) varies from 111 mm to 118 mm.

3.3 Impact Test Setup

The T-specimen, supplied by NAL Bangalore, is first impact by some energy and then it is subjected to pulling. Same setup as described in previous chapter for impact is also used to impact the T-specimen; only change that has been done for the impact of T-specimen is the Spacer bar (3) , shown in Fig. 3.2, is placed in between Front pressing plate (2) and Support Plate (7). The Spacer bar is used so as to provide a movable support at the back side of the specimen, such that the load acting on the specimen during impact is not transmitted to the plydrop region.

3.4 Pulling Test Fixture

The schematic diagram of T–pull setup is shown in Fig. 3.3. The flange of the T-joint is screwed to the Specimen Holder with eight M5 screws and its web is screwed to the Connector through two Web Plates. Specimen holder and Connector are mounted to the jaws of the Tensile Machine through a Hinge Fork on each sides.

To mount the flange of T-joint to the specimen holder (2), 8 holes of diameter 5.5 mm are drilled in the flange. Also 4 holes of diameter 5.5 mm are drilled in the web to mount it to the web plate (5).

To make the specimen holder, a vertical plate of 10 mm thickness is welded to the base plate (Fig. 3.4). In order to facilitate positioning of vertical plate on the base plate before welding, a 2 mm deep and 10 mm wide groove is made on the top surface of the base plate. The vertical plate is supported by 4 triangular webs as shown in Fig. 3.4. Again 2 mm deep grooves are made at the top surface of the base plate to position the web properly. Eight 5.5 mm diameter holes are drilled on the base plate to fasten the flange of the specimen to the specimen holder using M5 bolts. A 12.7 mm diameter hole is drilled and reamed on the centre line of the vertical plate; centre of the hole is at 25 mm

below the top edge. This hole is used to connect the base plate to the Hinge fork using a Pin.

The Specimen Holder is pinned to the Hinge Fork (3) with the help of Pin (4). Hinge fork is made from a mild steel cylindrical block with a slot cut in the bottom and a hole drilled on the top. Dimensions of the Hinge Fork is shown in Fig. 3.5. The slotted portion also has a hole drilled of 12.7 mm which is used to fasten the Connector and the Specimen holder with the help of the hardened pin. The upper hole is pinned to the jaws of the MTS. Since two pin joints, normal to each other, are provided in the design of the test fixture, only tensile force is transmitted to the T-pull specimen.

Diameter of pins used in this setup is 12.7 mm and their length is 90 mm. Dimensions of pin is shown in Fig. 3.6. They are made of alloy steel (EN24) hardened to 38 Rockwell C hardness.

The web of the T-joint is bolted to the Web Plate (5) with four M5 bolts which is pinned to the Hinge Fork through Connector (6) with the help of the Pin. The web plate is a rectangular and is made of mild steel. Two such plates are used to hold the web of the T-joint. There are eight holes of diameter 5.5 mm in the web plate, shown in Fig. 3.7.

Connector (6) is a rectangular plate with the top edge made thinner, shown in Fig. 3.8, to enable fit joint with the web plate along with the specimen. This section has four 5.5 mm diameter holes which are aligned with the holes on the web plates on being assembled. The lower half of the connector contains a hole drilled and reamed in it of diameter 12.7 mm.

This assembly is then supported between the jaws of the Material Test System with the help of two pins, shown in Fig. 3.9.

3.5 Preliminary Results

Only preliminary tests on T-pull specimen are conducted so far. The work is progressing at slow pace because the T-pull specimens are expensive and experiments are to be conducted in a reliable manner.

One T-pull specimen (web 2.90 mm thick and flange 79.72 mm in length) is impacted with 3.0 J. It is to be noted that the specimen should be aligned properly so that the centre of impact is in line of the centre of the web of the specimen. An alignment tool has been designed, fabricated and made functional for this purpose. The alignment tool worked well as the impact was found to be in line with the centre of the web of the specimen. Tension test has not been conducted on the impacted specimen as the damage has to be identified through a C-scan.

Tension test was carried out on an unimpacted T-pull specimen (web 2.96 mm thick and flange 79.86 in length). The failure occurred through initiation of delamination cracks at place inside the delta region of the T-joint (fig. 3.10). One of the cracks moved up inside the web. Other interlaminar crack moved into the flanged portions on each of the delta triangle. The load versus displacement of this specimen is shown in Fig. 3.11. The plot of load-displacement is linear up to 5.9 kN where the failure of the specimen took place. The load then was suddenly reduced.

During testing it was observed that the centre of the flange of the T-pull specimen separated from the specimen holder, shown in Fig. 3.10. The specimen's flange is bolted to the specimen holder through two rows of bolts; the rows are separated by a distance 105 mm to avoid drilling holes in the plydrop region of the T-pull specimen. This distance is quite large and the pulling force makes the flange bow out creating a gap of about 2.75 mm at the failure. The bending of the flange infact changes the geometry of the specimen, thus raising questions whether the test is valid. Some future experimentation may be tried with reduced distance between the two rows of the bolts. Then the hole will be made in the plydrop portion of the joint. After the test, one may study whether the fracture starts from the drilled holes. If the failure does not initiate at the drilled holes, the test will considerably reduce the bowing of the specimen.

3.6 Closure

The experimental setup has been developed successfully and preliminary tests have been carried out with the setup. The work presented in this chapter consists of description and development of setup, dimensions of different

parts of setup and preliminary results. A tension test was conducted on an unimpacted T-pull specimen (web 2.96 mm thick and flange 79.86 in length).

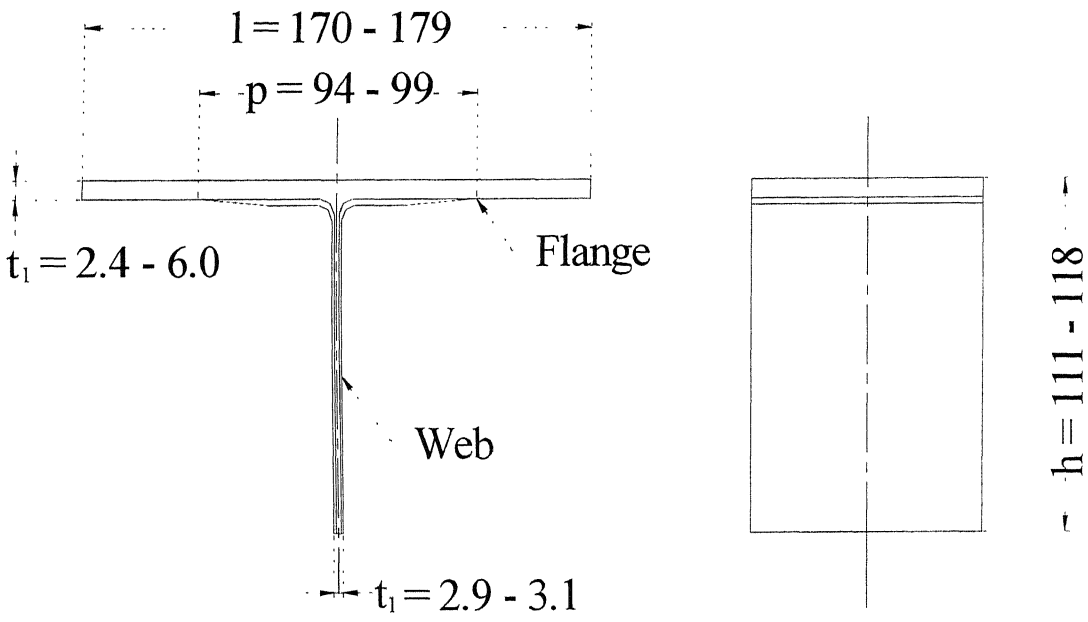

Fig. 3. 1 T-Pull Specimen (Supplied by NAL Bangalore)

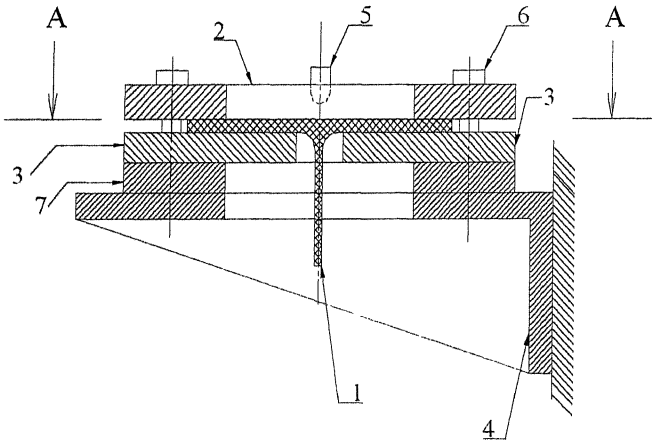

1. Specimen
2. Front Pressing Frame
3. Spacer Bar
4. Mounting Frame
5. Striker Bar
6. Clamping Capscrews
7. Support Plate

Fig 3. 2 Schematic diagram of impact setup for T-specimen

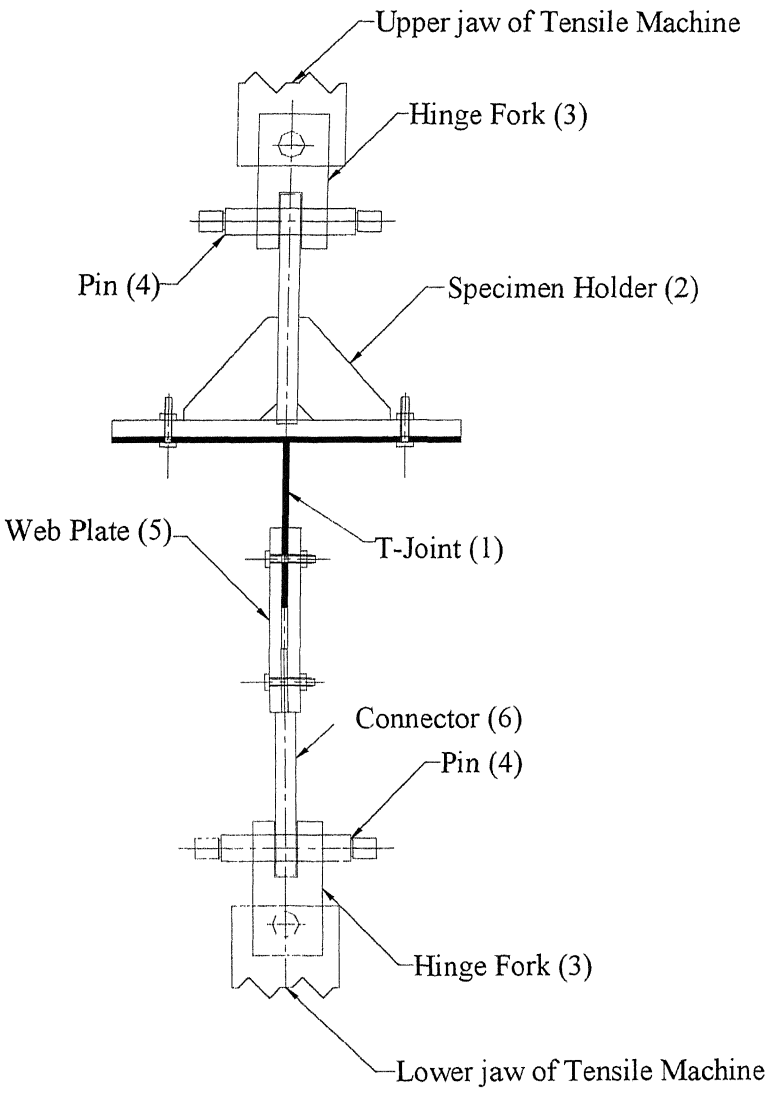

Fig. 3. 3 Schematic Diagram of T-Pull setup

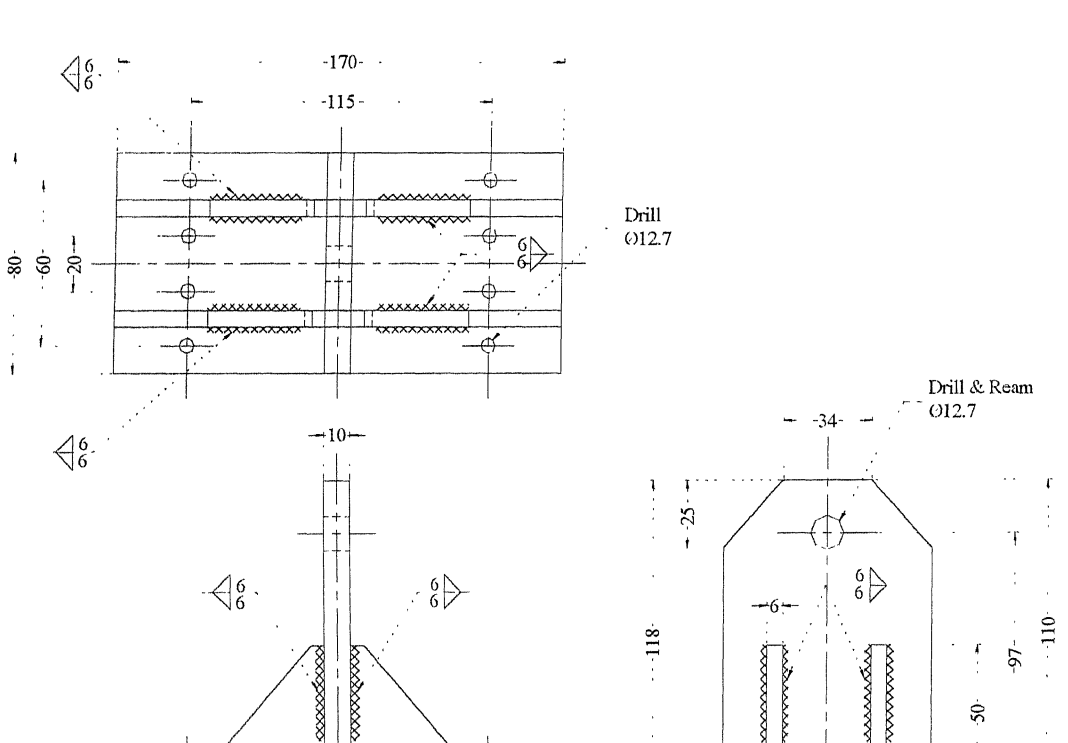

Fig. 3. 4 Specimen Holder

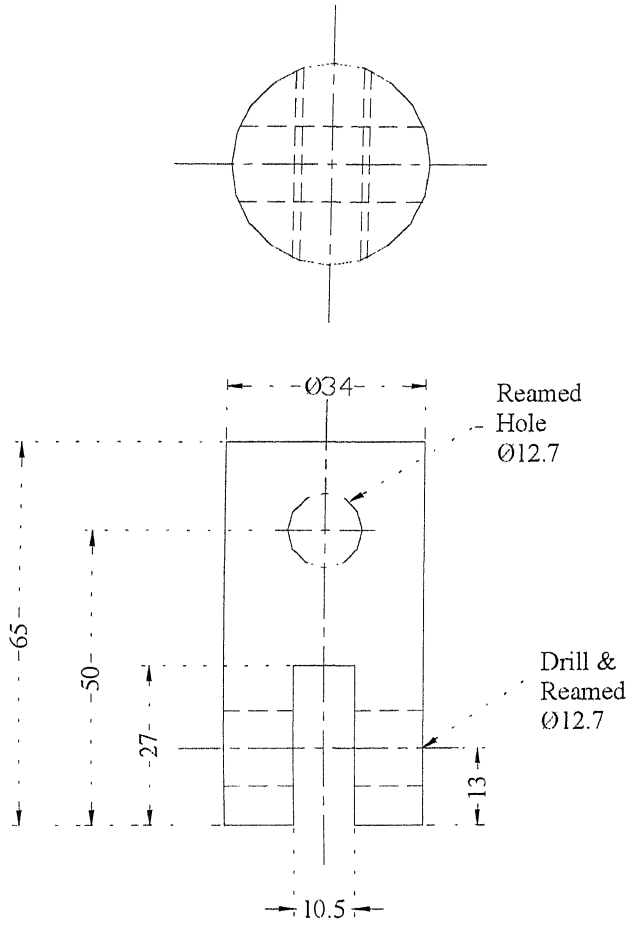

Fig. 3. 5 Hinge Fork

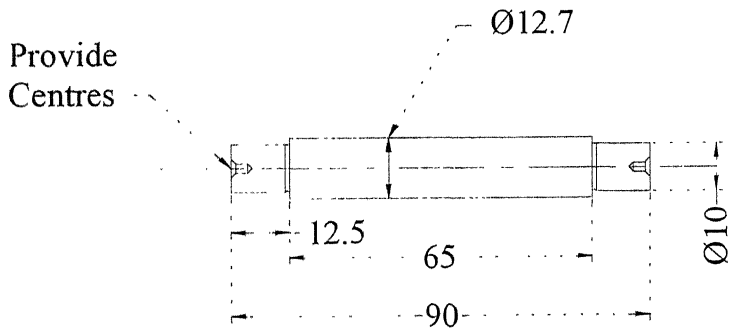

Fig. 3. 6 Pin

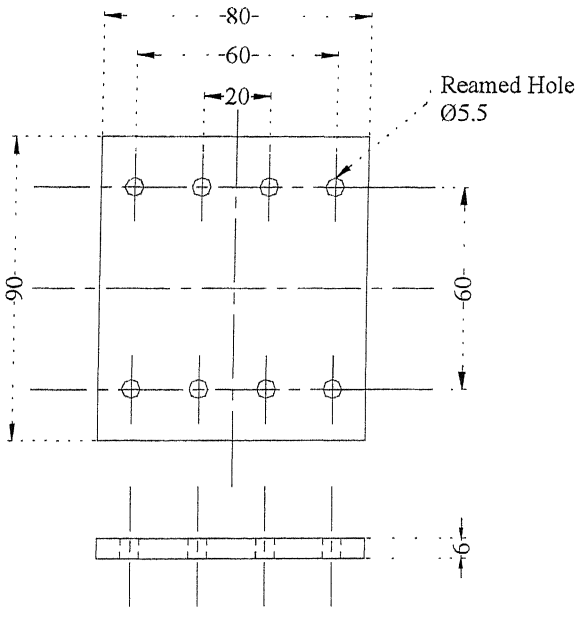

Fig. 3.7 Web Plate

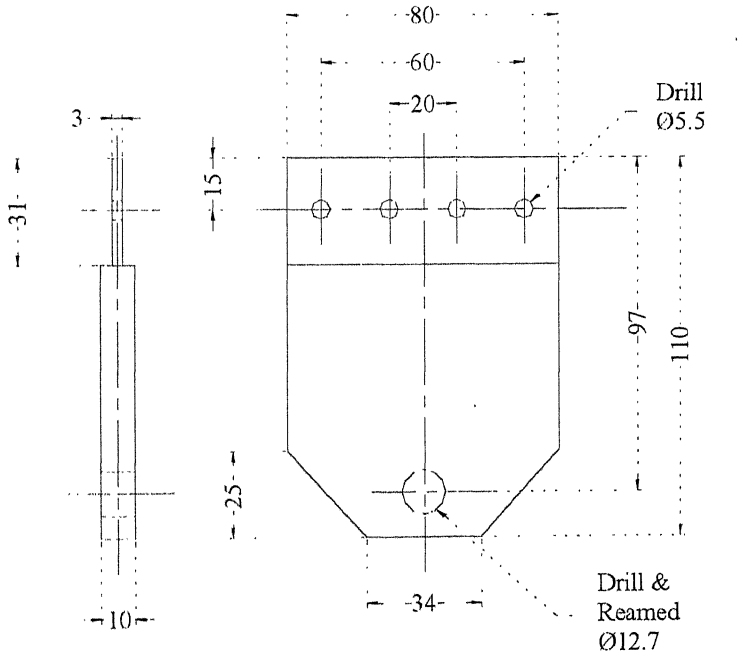

Fig. 3. 8 Connector

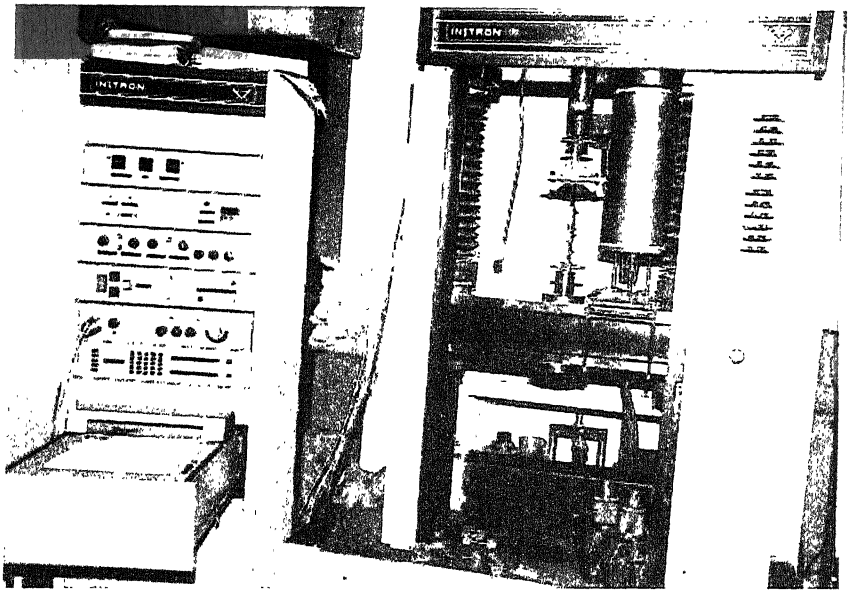

Fig. 3.9 Photograph Showing T-Pull specimen holds between the jaws of MTS

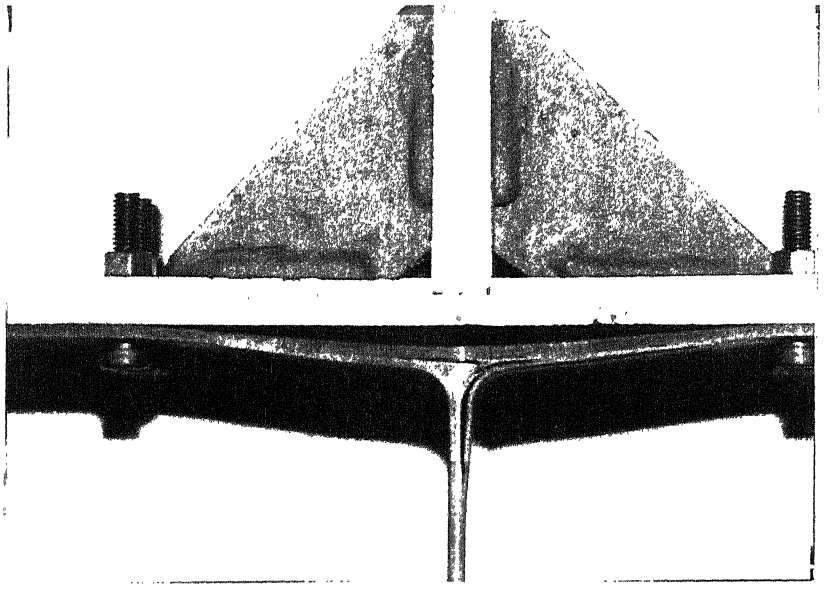

Fig. 3.10 Photograph showing the failure of T-pull specimen during Tension test

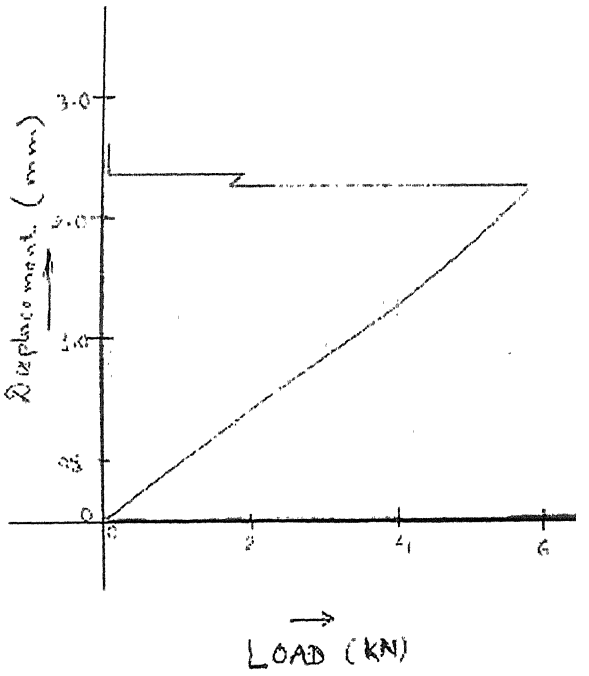

Fig. 3.11 Load-Displacement plot of an unimpacted T-pull specimen

Chapter 4

Results and Discussion

Compression After Impact Experiment

4.1 Introduction

Tests to determine Compression after Impact (CAI) strength of composite laminates are carried out. The specimens of composite laminates with two configurations are used for performing the CAI tests:

- $[0/45/-45/90/90/-45/45/0]_{2s}$, Glassfiber Angleply Laminate (GAL)
- $[0]_{24}$, Glass Fiber reinforced epoxy Laminate (GFL).

The specimens were first impacted with 12 J (approximately) with the help of the airgun setup described in Chapter 2. Then the impacted panels were subjected to compression test.

4.2 Impact Test

The specimens were impacted in controlled conditions, with the help of an airgun setup described earlier. The striker bar used in these experiments was made of aluminium; length of striker used was 15.5 mm(approximately), shown in

Fig. 2.4; its diameter was 12.6 mm (approximately) and its mass varied between 4.7 gm and 5.0 gm.

The specimen was first clamped in between the rear mount plate and the front mount plate. The gas chamber was then filled with compressed air and released with the help of the solenoid valve. The striker was accelerated in the gun barrel and impacted the specimen. Velocity of the striker was measured with the help of a laser torch and oscilloscope as described in Chapter 2. Details of impact test (impactor mass, impact velocity and impact energy) on the specimens are given in Table 4.1 and Table 4.2. Each specimen was impacted with 12 J (approximately).

4.3 Compression Test

The impacted specimens were prepared for compression test as described in Chapter 2. They were then clamped along with buckling the guides between the jaws of the MTS to find their compressive strength. The strain gauges, attached on both sides of the specimen, were connected to virtual instrumentation. The specimen was then compressed under displacement controlled mode with the loading rate of 4 mm/min. The load was applied till the specimen failed completely, i.e. upto the moment the specimen was unable to bear any load. The data obtained was then plotted using GNUPLOT. The GFL specimen (F1) after compression failure is shown in Fig. 4.1(b) and its stress-strain plot is shown in Fig. 4.1 (a). The dimensions of the specimen were 100 mm $\times$ 150 mm and strain gauges were attached at the positions described in Fig. 2.13 In Fig. 4.1(b) only one strain gauge can be seen; other strain gauge is aligned with the first but at the reverse side of the specimen. Four end tabs, as shown in the Fig. 4.1(b), are of dimension 100 mm $\times$ 60 mm; they are attached to the specimen for its proper gripping in the jaws of MTS. The area enclosed by blue pen shows the damage area due to impact and the damage extending laterally being shown by area bounded between two green lines.

In the plot, shown in Fig. 4.1(a), the responses of both the strain gauges being same at the initial stage upto 42 MPa. Then the strain curves start deviating from each other showing that the specimen buckles in spite of using buckling guides. The deviation is due to the increase of buckling; the

magnitude of compressive stress of one side (ϵ_1) increases and decrease on the other side (ϵ_2). Infact, at high compressive stress of 66 MPa response of one of the strain gauge (ϵ_2) becomes tensile.

4.3.1 Criterion for Compressive Strength

In the plot, shown in Fig. 4.1(a), it is found that after a certain load, strain increases on one side and decreases on the other side due to buckling of the specimen. Some criterion should be chosen to evaluate the compressive strength of the specimens. To evaluate the compressive strength of the specimens a criterion is formulated in this study which is based on the fact that the difference between strains on two sides of a panel is equal to 20% of the average strain. Quantitavily, the criterion is:

$$\left[\frac{\epsilon_2 - \epsilon_1}{\left(\frac{\epsilon_1+\epsilon_2}{2}\right)}\right] = 0.2$$

The failure of specimen is taken at the point where it follows the above mentioned failure criterion and the compressive strength at that point is considered as the failure compressive strength.

4.3.2 Compressive Strength of GFL Panels

The failure of GFL specimens occurred in three distinct ways (Fig. 4.1 to 4.10). In the first type of failure the impacted damage area extended to both the side edges of the specimen. Specimens F1, F4, F5 and F7 failed through this kind of failure. In the second category of failure, the damage due to impact extended to only one side; Specimens F3, F6, F8, F9 and F10 lie in this category of failure. In the third category of failures, the failure during compression took place at a location which is slightly far away from the centre of the impact. Specimen F2 failed through this category.

According to the failure criterion, discussed in previous section, compressive strength of the specimen shown in Fig. 4.1 was 45.9 MPa. Compressive strength of other GFL specimens shown in Fig. 4.2 to Fig. 4.10 are given in Table 4.3. The average compressive strength of failure of GFL

specimens was 58.5 MPa.

4.3.3 Compressive Strength of GAL Panels

The failure of GAL specimens occurred in two distinct ways. In first type of failure the damage area due to impact extended to both sides of the specimen, the specimens A1, A2, A3 and A4 lie in this category of failure. In second category of failure the damage due to impact extended to only one side; specimen A5 lie in this category of failure. These specimens can be seen in Fig. 4.11 to Fig. 4.15. The compressive strength of GAL specimens, after satisfying the failure criterion mentioned in previous section, is given in Table 4.4. The average compressive strength of failure of GAL specimens is 15.7 MPa.

4.3.4 Discussion

From the results of both GFL and GAL specimens (given in tables 4.3 and 4.4), it is observed that in comparision to GAL specimen the GFL specimens possess much higher compression strength after impact. The average compressive strength of GFL specimen is 58.5 MPa which is 3.7 times higher than the compressive strength of GAL specimen. All panels of GFL and GAL were impacted with the impact energy close to 12 J and similar striker bar made of aluminium. The impact damage area in GFL and GAL panels is similar. However, the growth of damage area under compressive load shows that failure zone is wider in case of GAL. This suggests that delamination cracks in a laminate already nucleated by impact of a foreign body propagate more easily in angleply laminates. This matches with the finding of Kumar and Rai (1990) that replacement of the surface ply on each side of an angle plied Kavlar reinforced epoxy laminate with a balanced ply of fabric reduced the projected impact damage area. This might also explain that interlaminar cracks of GAL specimen reach the side edges of the specimen at much reduced load.

4.4 Closure

The compression after impact tests conducted on two type of specimens, glassfiber fabric laminate and glassfiber angleply laminate. It was found that compressive strength of glassfiber fabric laminate is 3.7 times the compressive strength of glassfiber angleply laminate as the average compressive strength of glassfiber fabric laminate specimens is 58.5 MPa and the average compressive strength of glassfiber angleply laminate specimen is 15.7 MPa. This means that the GFL specimens are better than the GAL specimens in CAI test.

Table 4.1: Details of the Impact Test of GFL specimens

Exp. No.	Striker Mass (gm)	Impact Velocity (m/s)	Impact Energy (J)
F1	4.7780	71.02	12.05
F2	4.8601	70.01	11.91
F3	4.8428	69.02	11.60
F4	4.8428	71.10	12.24
F5	4.8521	69.40	11.70
F6	4.8521	70.67	12.12
F7	4.8521	71.01	12.23
F8	4.8053	70.63	11.98
F9	4.8950	69.73	11.90
F10	4.8950	70.64	12.21

Table 4.2: Details of the Impact Test of GAL specimens

Exp. No.	Striker Mass (gm)	Impact Velocity (m/s)	Impact Energy (J)
A1	4.8950	70.01	12.11
A2	4.8950	69.73	11.90
A3	4.8601	70.00	11.91
A4	4.7780	71.02	12.06
A5	4.7846	70.36	11.84

Table 4.3: Compressive Strength of GFL specimens at failure

Exp. No.	Compressive Strength (MPa)	Average Compressive Strength (MPa)
F1	45.9	58.5 ± 19.1
F2	90.1	
F3	84.3	
F4	32.1	
F5	62.2	
F6	68.4	
F7	64.2	
F8	51.4	
F9	52.2	
F10	34.6	

Table 4.4: Compressive Strength of GAL specimens at failure

Exp. No.	Compressive Strength (MPa)	Average Compressive Strength (MPa)
A1	14.2	15.7 ± 2.2
A2	15.3	
A3	17.3	
A4	13.2	
A5	18.6	

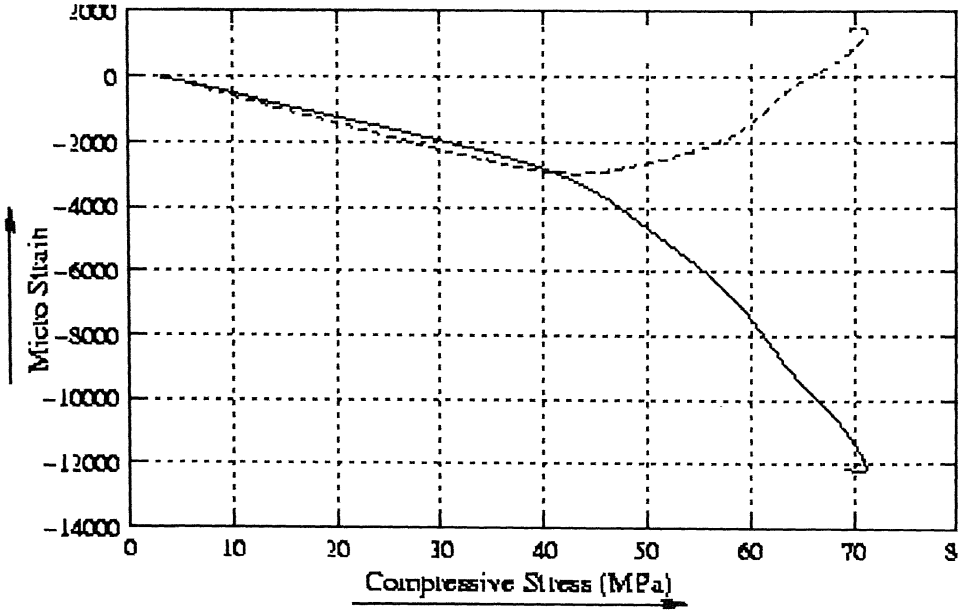

(a)

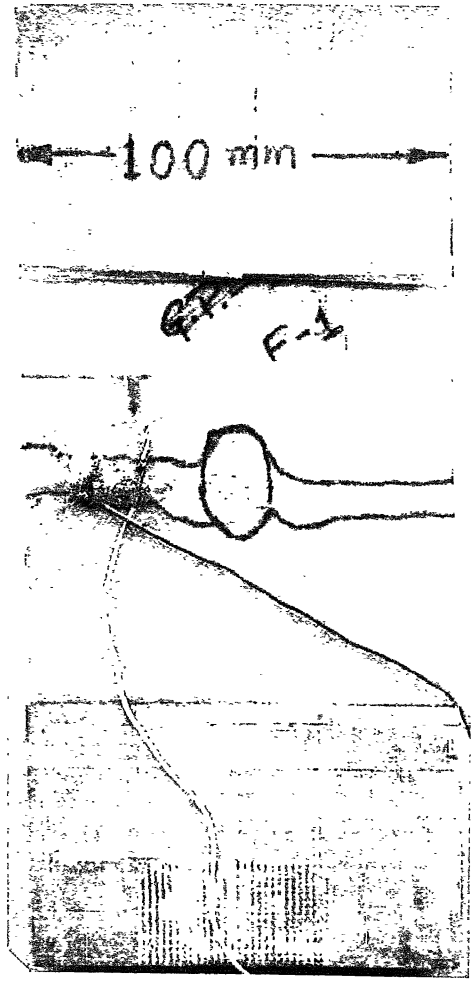

(b)

Fig. 4.1 GFL specimen (F1), with impact energy of 12.05 J;
(a) Stress vs. strain on front and rear strain gauges and
(b) Specimen after compression failure; damage area after impact is shown in blue and damage during compression is shown in green.

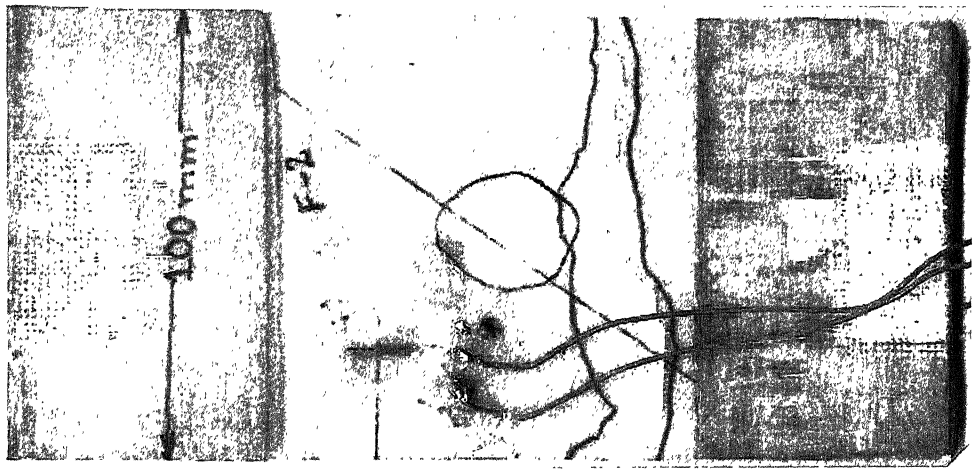

(b)

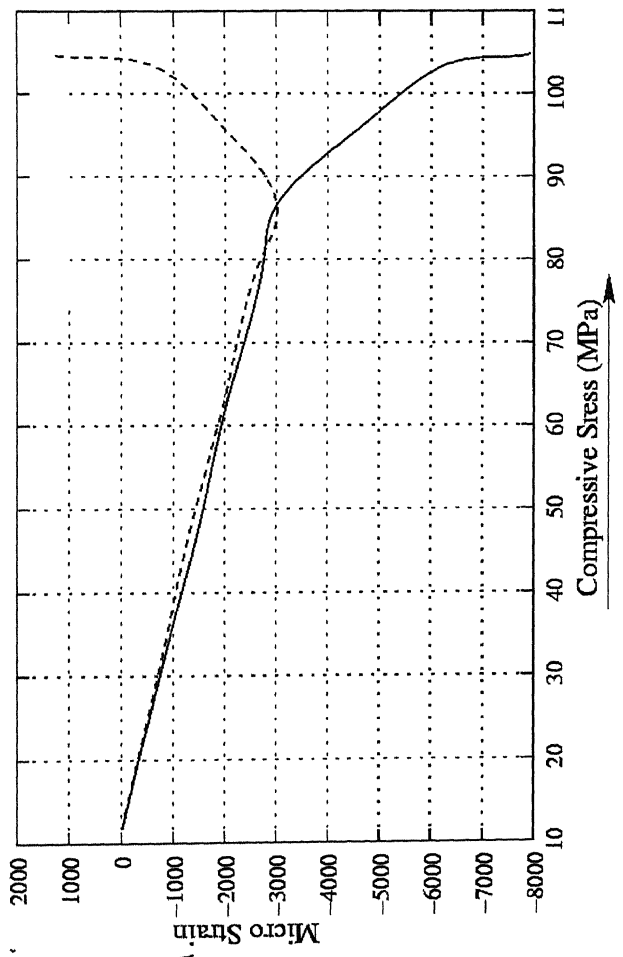

(a)

Fig. 4.2 GFL specimen (F2), with impact energy of 11.91 J; (a) Stress vs. strain on front and rear strain gauges and (b) Specimen after compression failure; damage area after impact is shown in blue and damage during compression is shown in green.

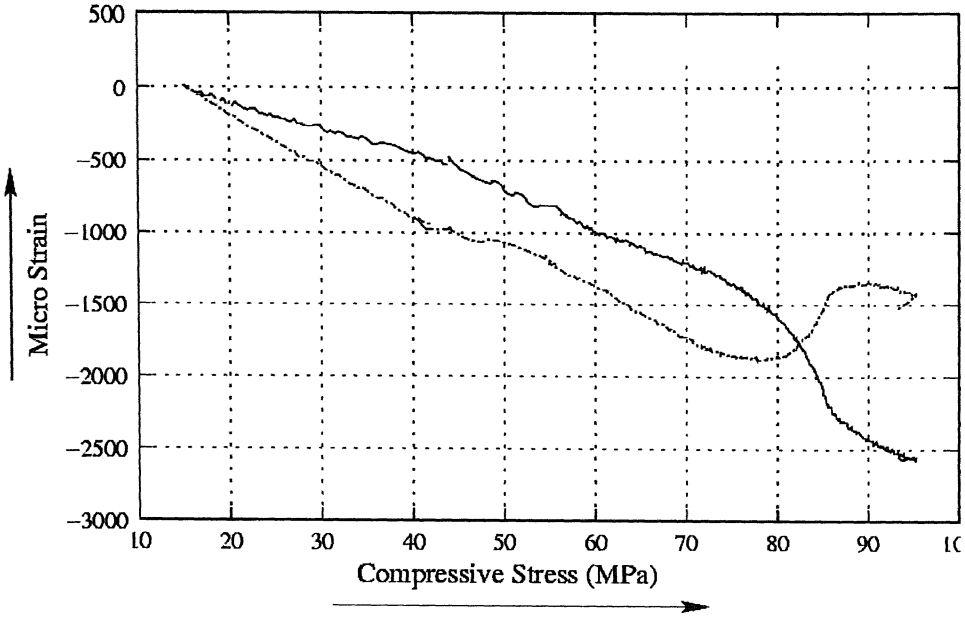

(a)

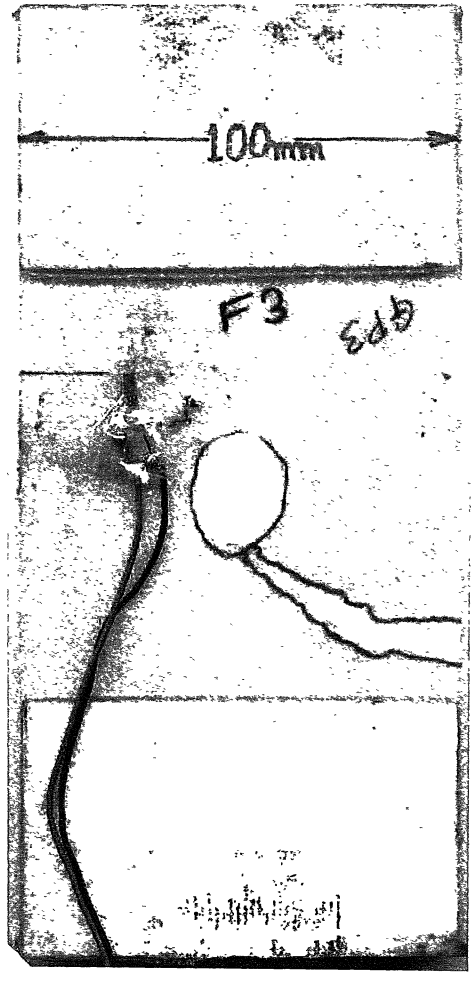

(b)

Fig. 4.3 GFL specimen (F3), with impact energy of 11.60 J;
(a) Stress vs. strain on front and rear strain gauges and
(b) Specimen after compression failure; damage area after impact is shown in blue and damage during compression is shown in green.

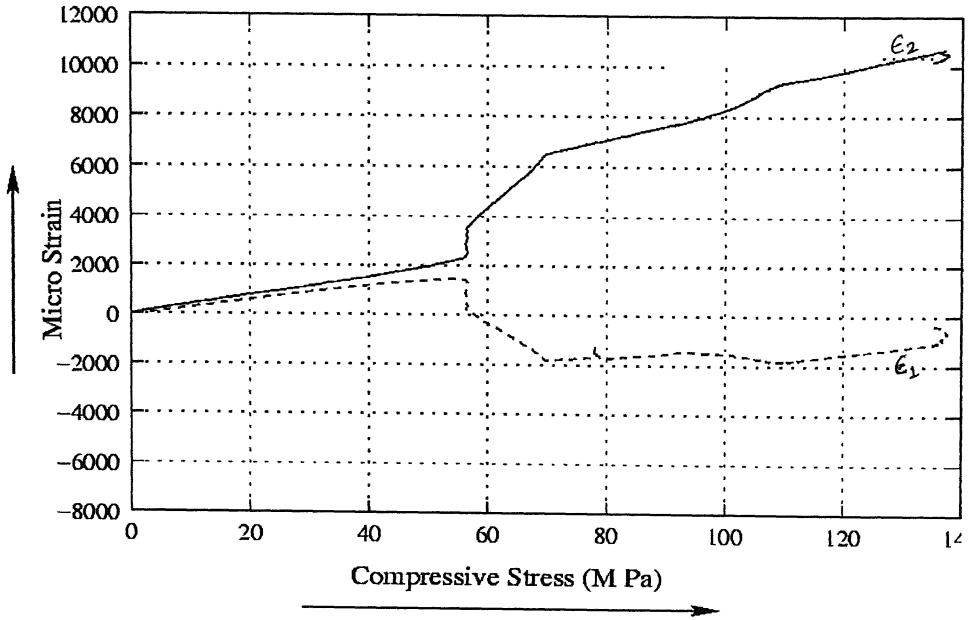

(a)

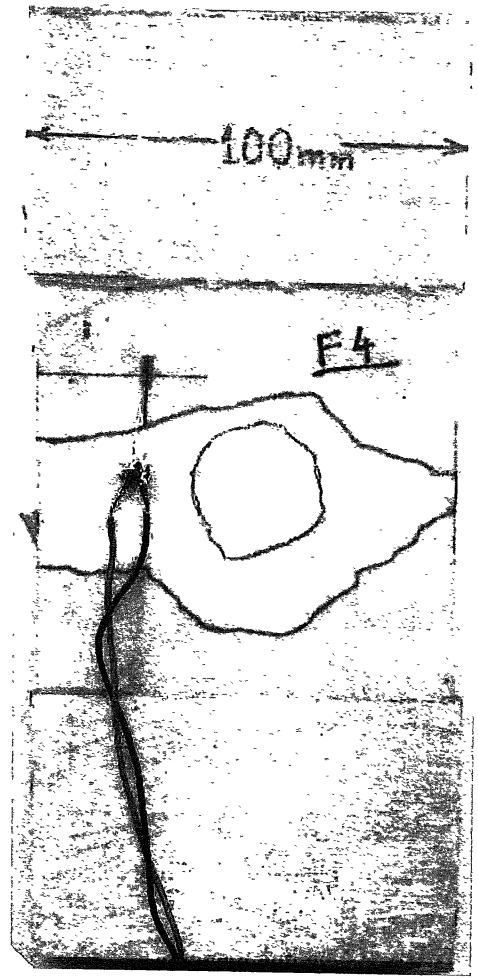

(b)

Fig. 4.4 GFL specimen (F 4), with impact energy of 12.24 J;
(a) Stress vs. strain on front and rear strain gauges and
(b) Specimen after compression failure; damage area after impact is shown in blue and damage during compression is shown in green.

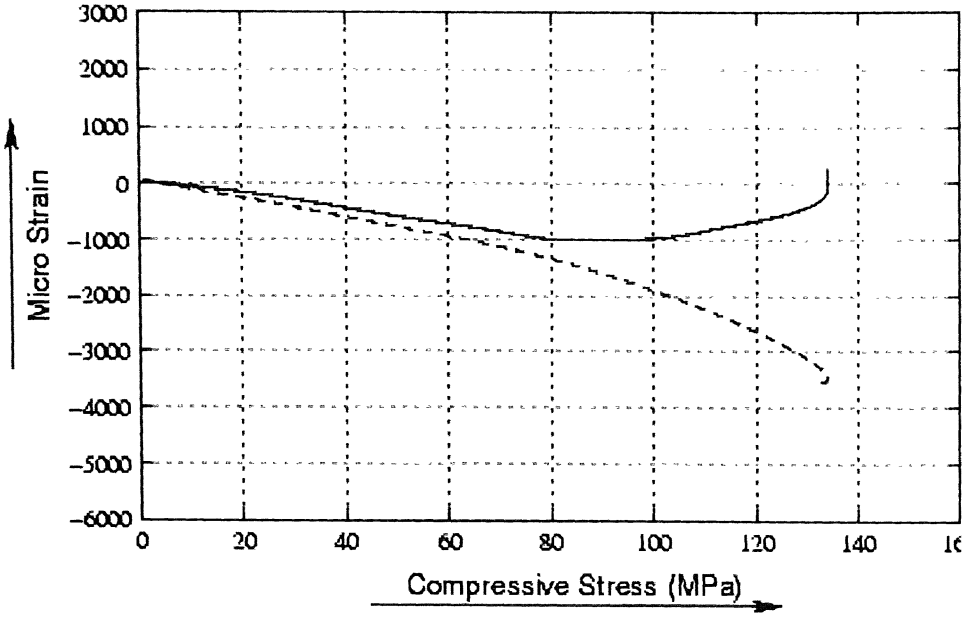

(a)

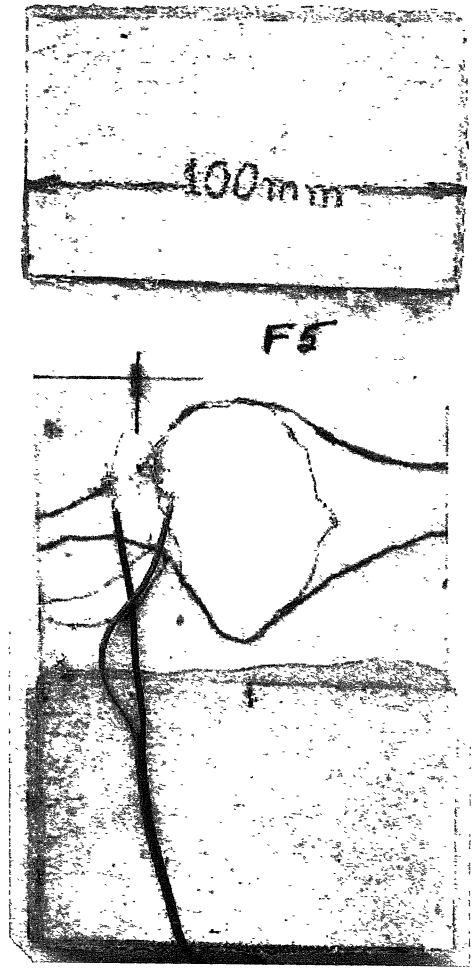

(b)

Fig. 4.5 GFL specimen (F5), with impact energy of 11.70 J;
(a) Stress vs. strain on front and rear strain gauges and
(b) Specimen after compression failure; damage area after impact is shown in blue and damage during compression is shown in green.

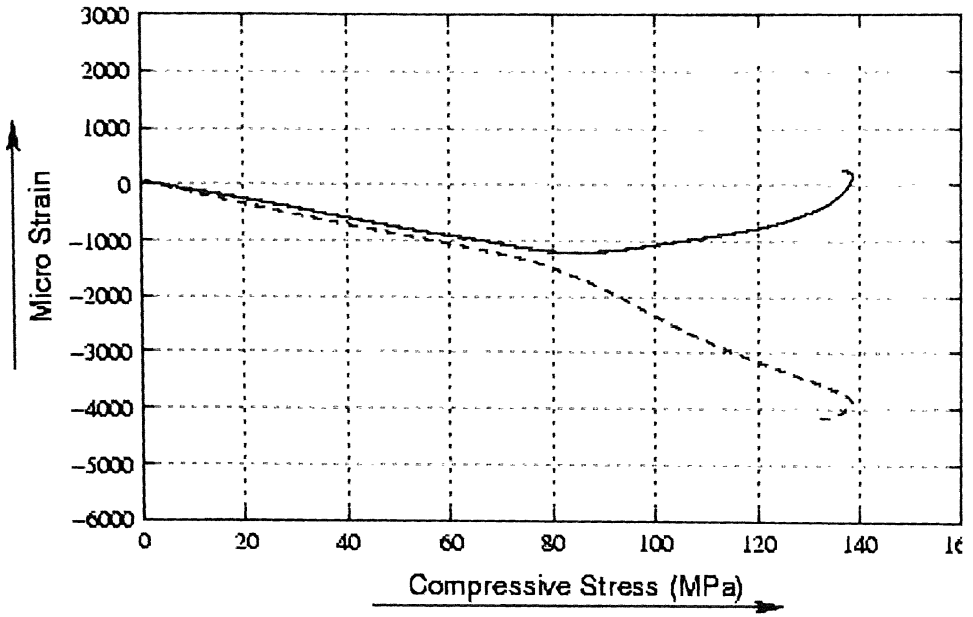

(a)

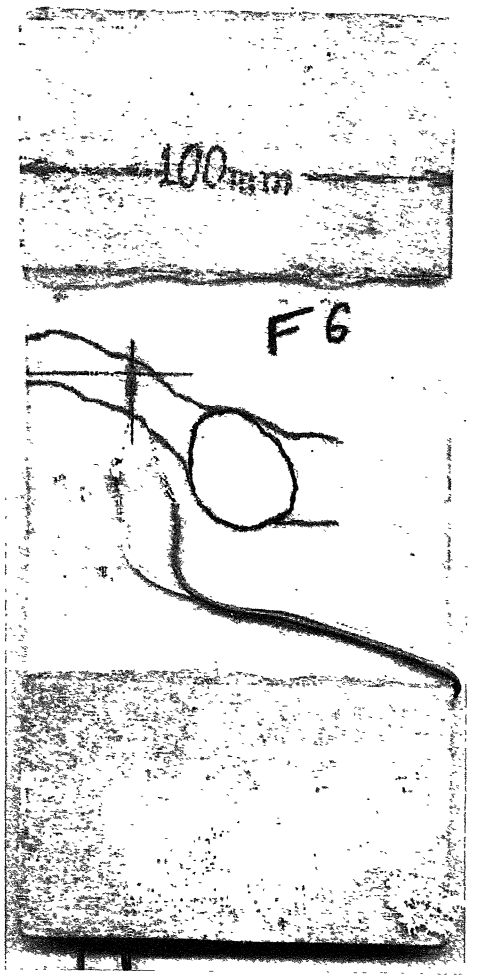

(b)

Fig. 4.6 GFL specimen (F 6), with impact energy of 12.12 J;
(a) Stress vs. strain on front and rear strain gauges and
(b) Specimen after compression failure; damage area after impact is shown in blue and damage during compression is shown in green.

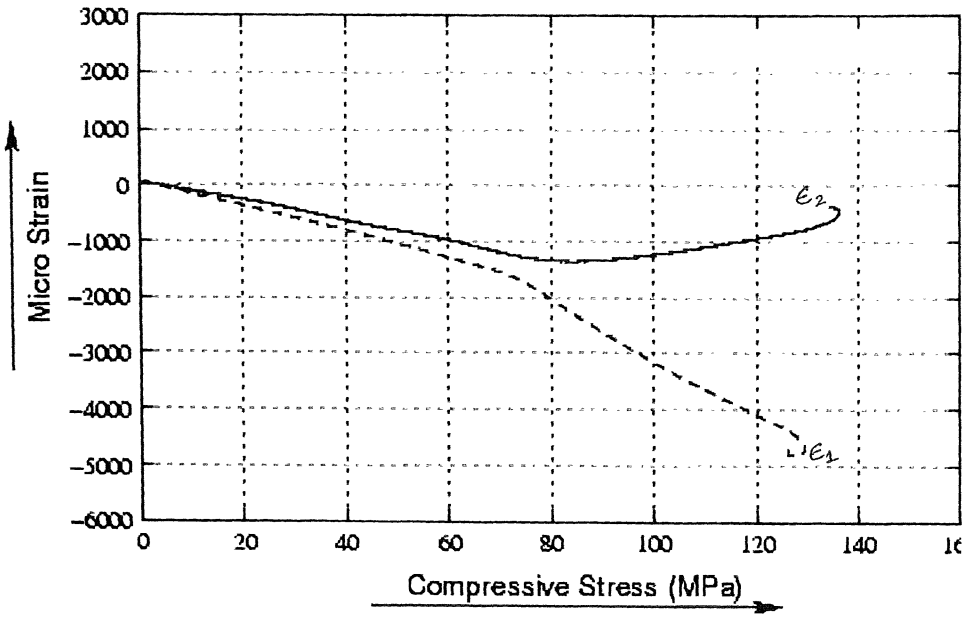

(a)

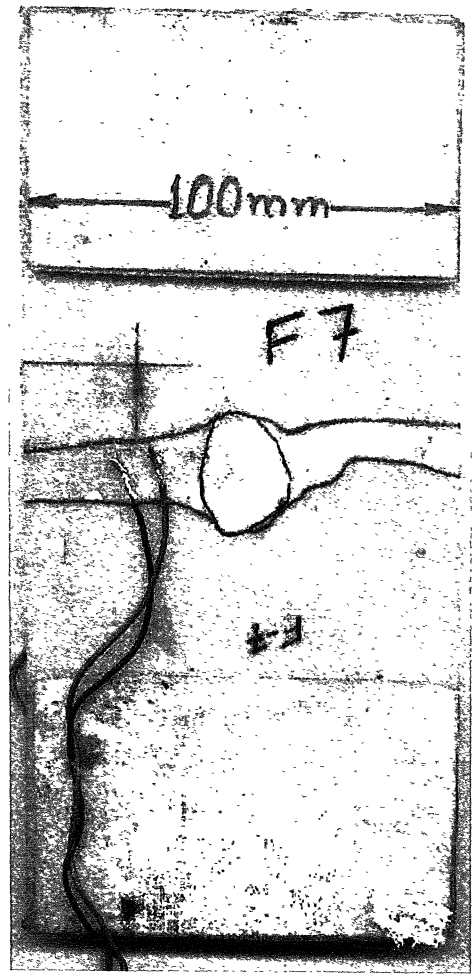

(b)

Fig. 4.7 GFL specimen (F 7), with impact energy of 12.23 J;
(a) Stress vs. strain on front and rear strain gauges and
(b) Specimen after compression failure; damage area after impact is shown in blue and damage during compression is shown in green.

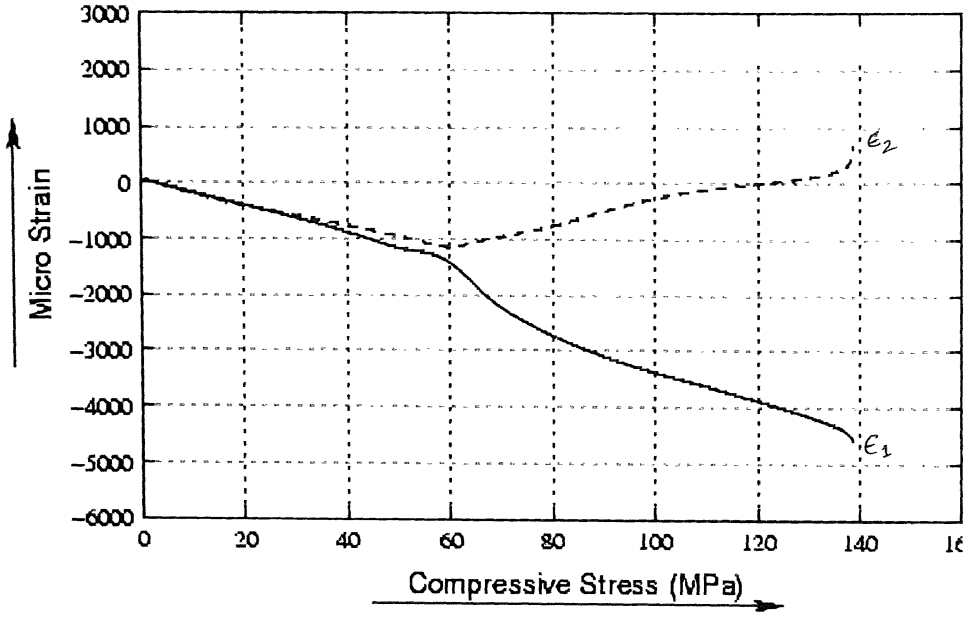

(a)

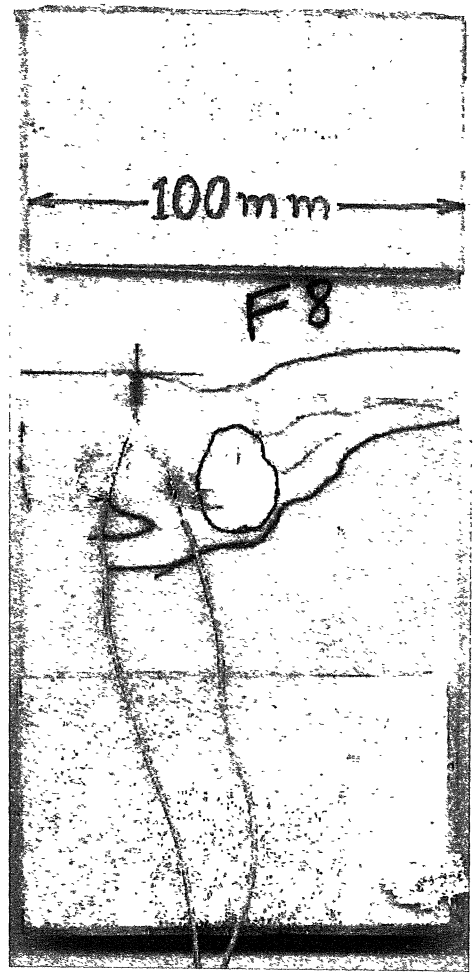

(b)

Fig. 4.8 GFL specimen (F 8), with impact energy of 11.98 J;
(a) Stress vs. strain on front and rear strain gauges and
(b) Specimen after compression failure; damage area after impact is shown in blue and damage during compression is shown in green.

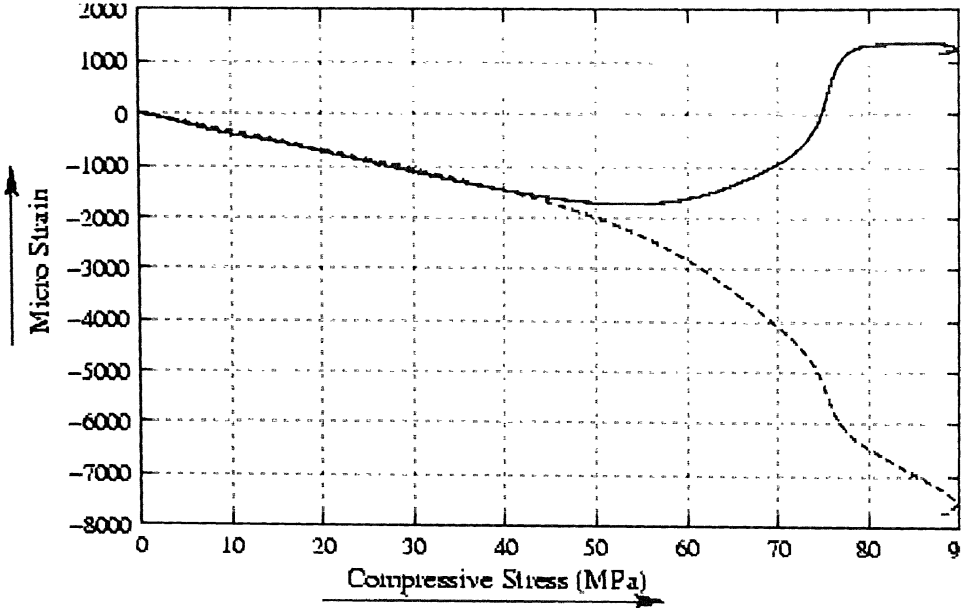

(a)

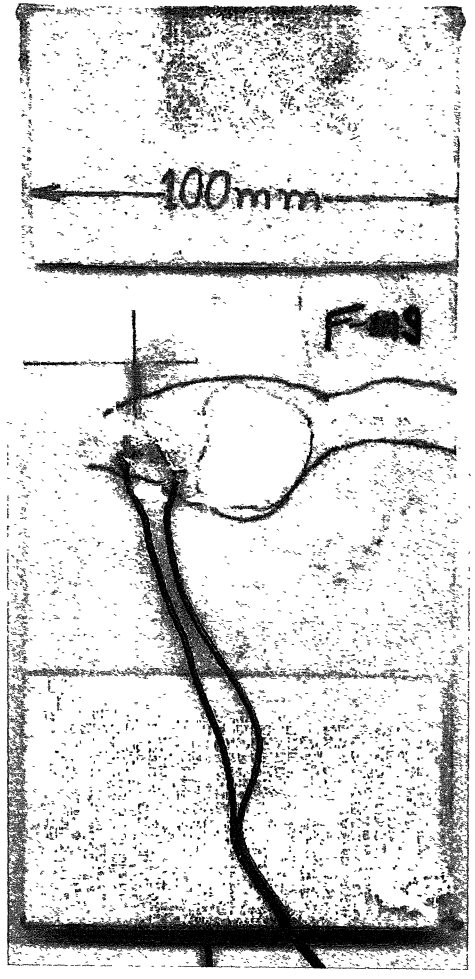

(b)

Fig. 4.9 GFL specimen (F9), with impact energy of 11.90 J;
(a) Stress vs. strain on front and rear strain gauges and
(b) Specimen after compression failure; damage area after impact is shown in blue and damage during compression is shown in green.

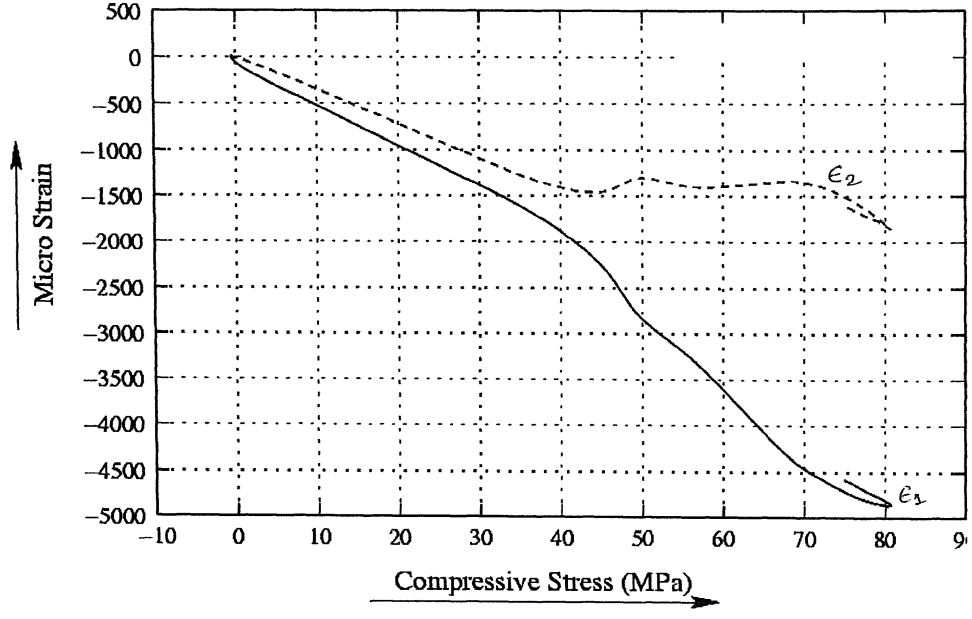

(a)

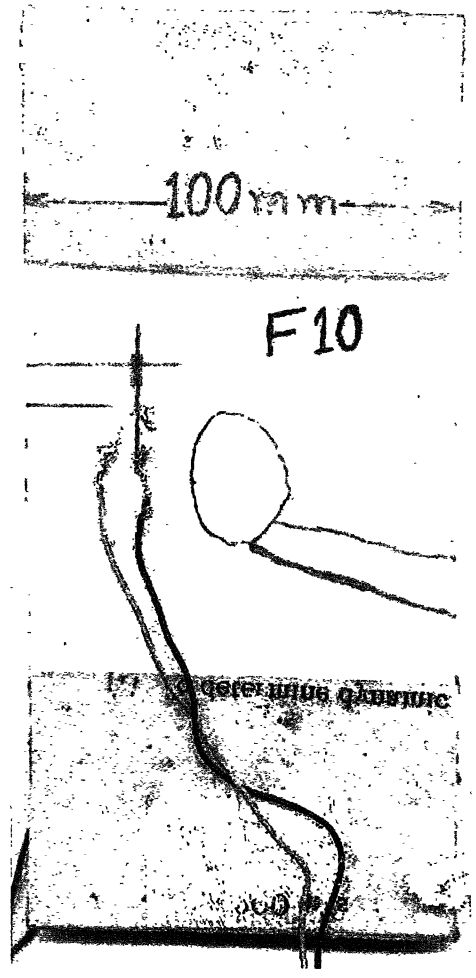

(b)

Fig. 4.10 GFL specimen (F 10), with impact energy of 12.21 J;
(a) Stress vs. strain on front and rear strain gauges and
(b) Specimen after compression failure; damage area after impact is shown in blue and damage during compression is shown in green.

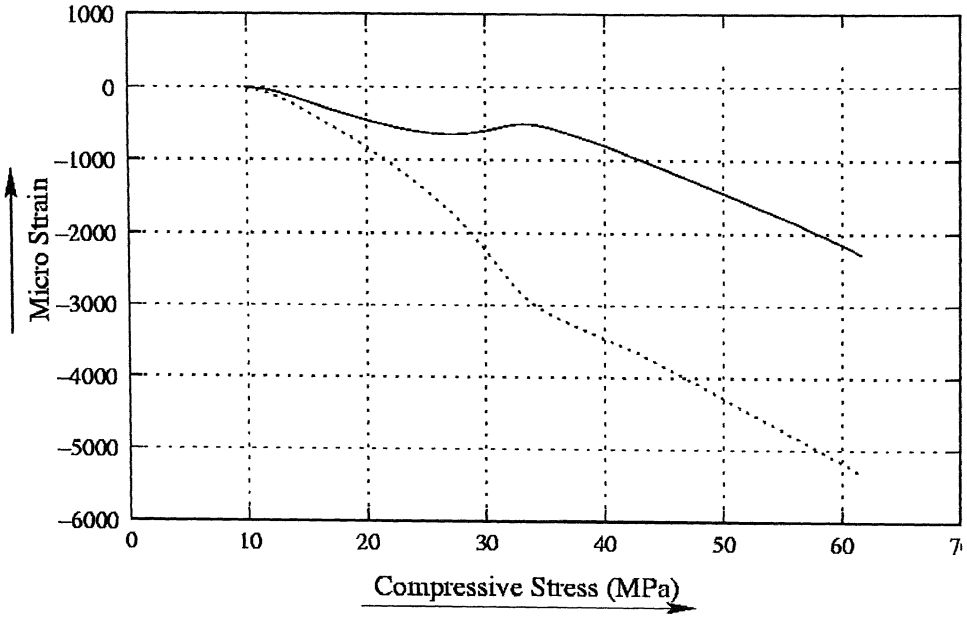

(a)

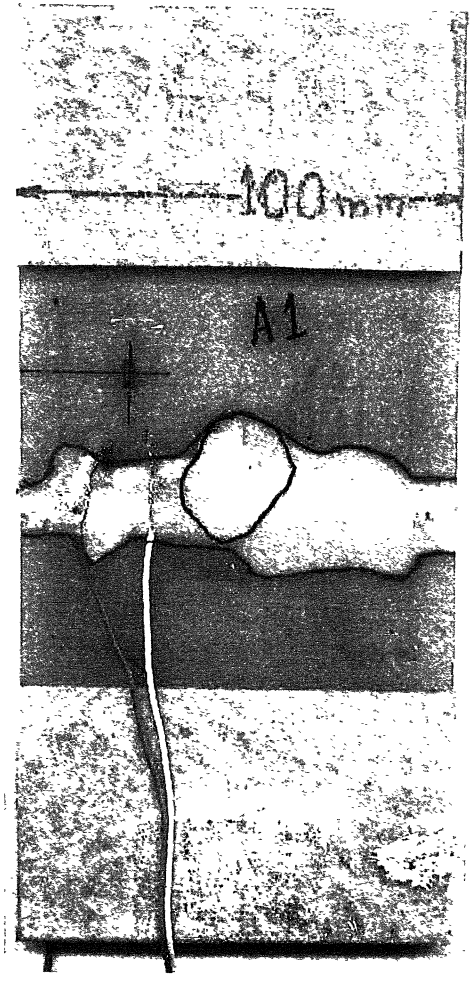

(b)

Fig. 4.11 GAL specimen (A1), with impact energy of 12.11 J;
(a) Stress vs. strain on front and rear strain gauges and
(b) Specimen after compression failure; damage area after impact is shown in blue and damage during compression is shown in green.

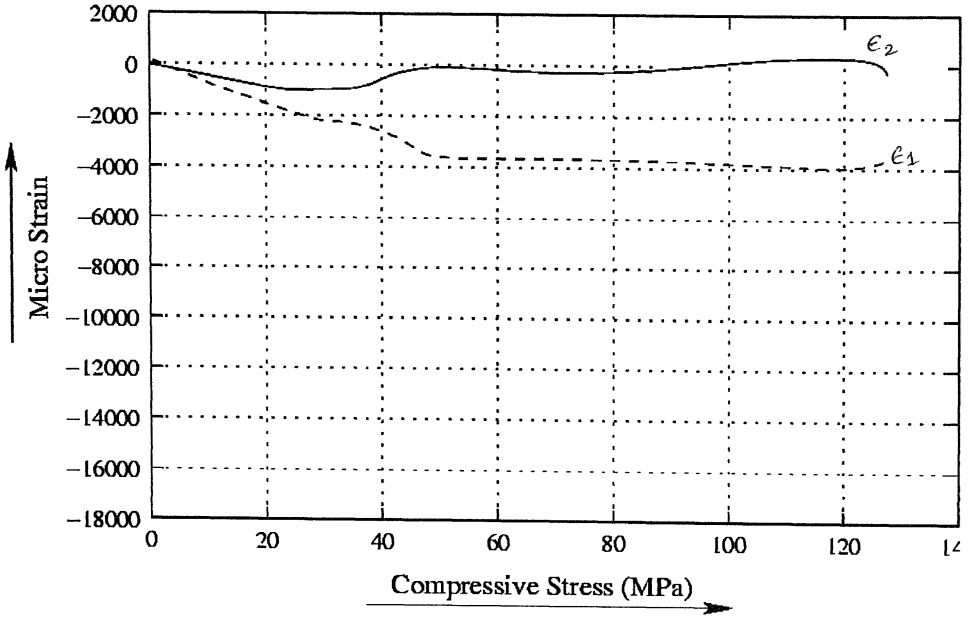

(a)

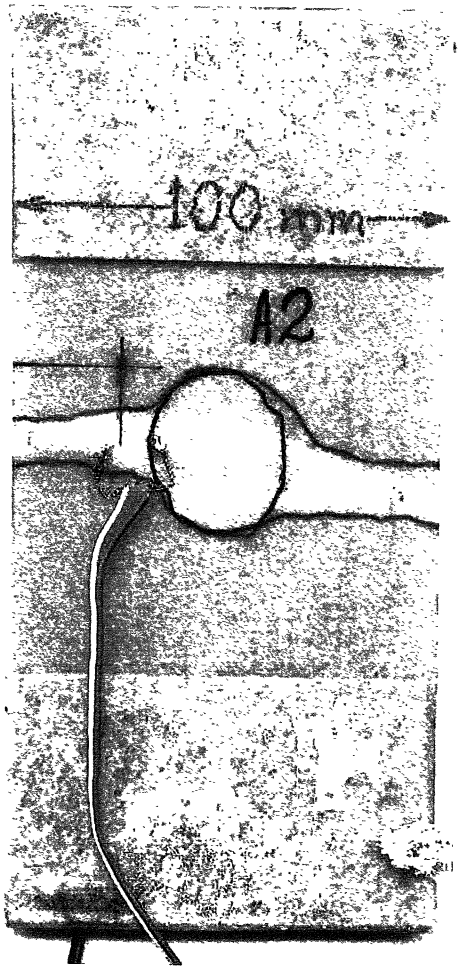

(b)

Fig. 4.12 GAL specimen (A 2), with impact energy of 11.90 J;
(a) Stress vs. strain on front and rear strain gauges and
(b) Specimen after compression failure; damage area after impact is shown in blue and damage during compression is shown in green.

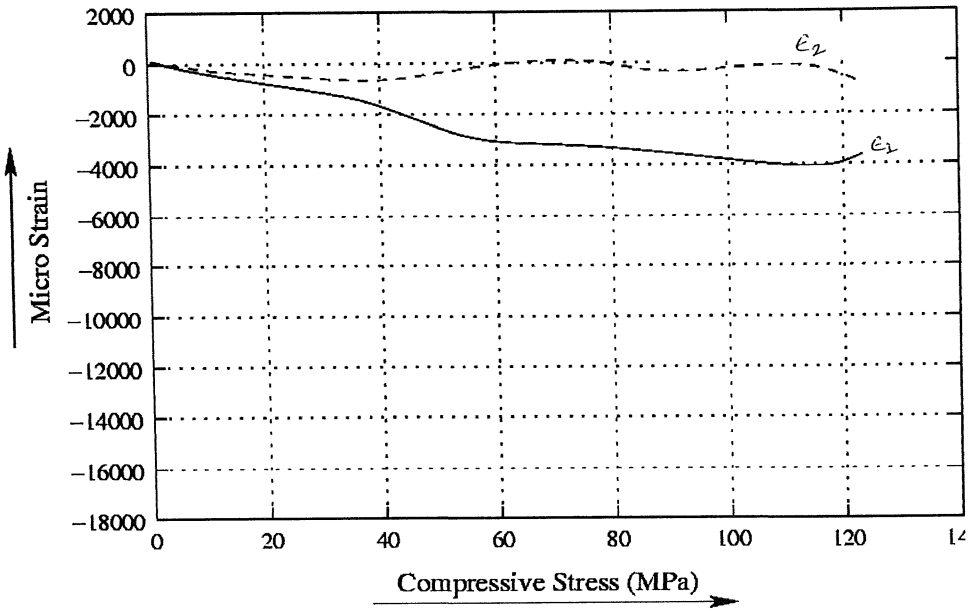

(a)

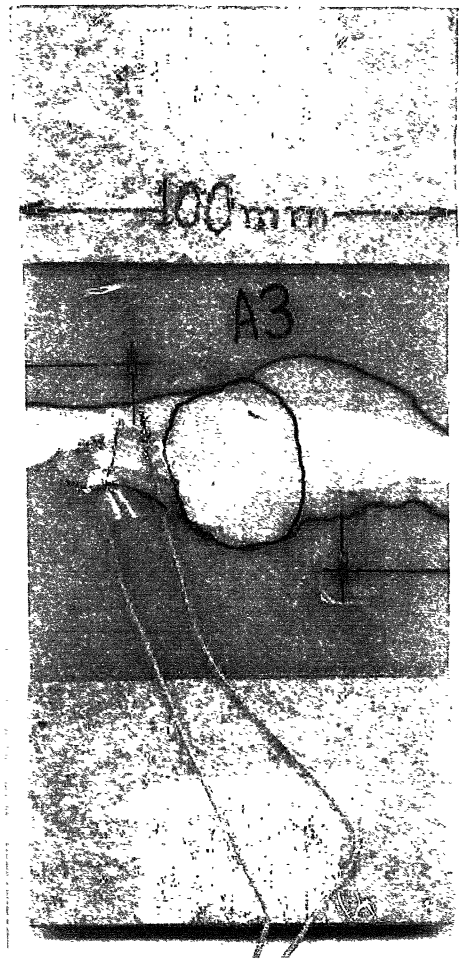

(b)

Fig. 4.13 GAL specimen (A 3), with impact energy of 11.91 J;
(a) Stress vs. strain on front and rear strain gauges and
(b) Specimen after compression failure; damage area after impact is shown in blue and damage during compression is shown in green.

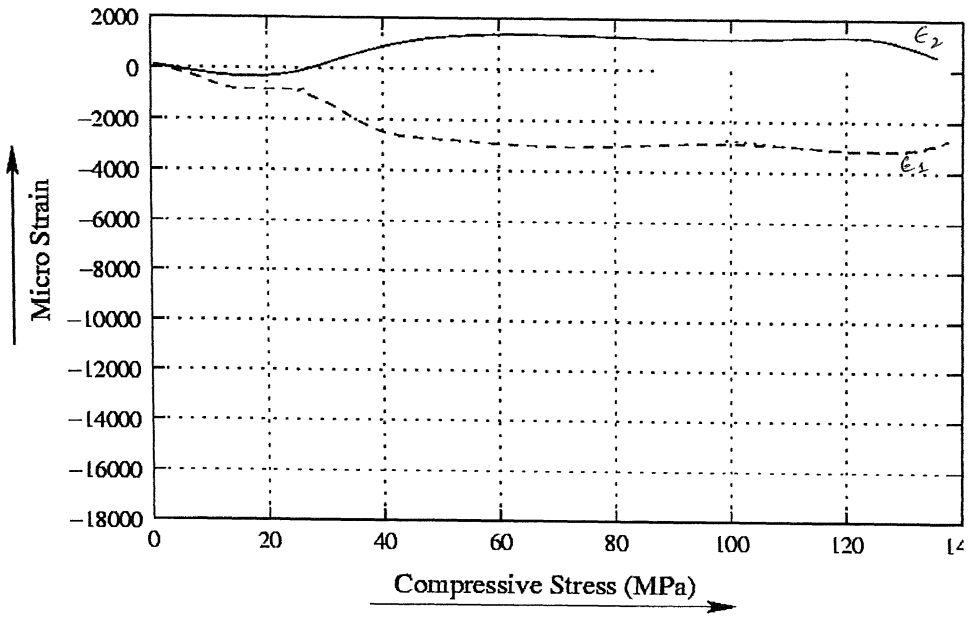

(a)

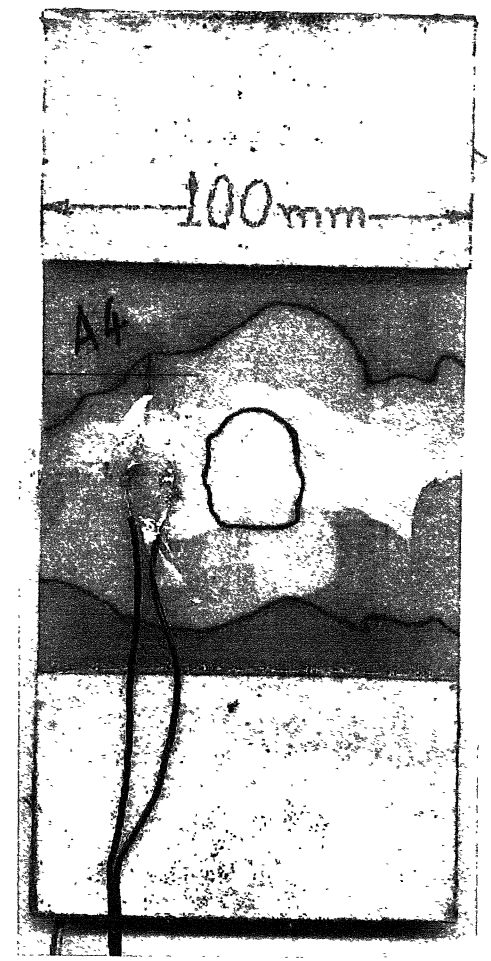

(b)

Fig. 4.14 GAL specimen (A 4), with impact energy of 12.06 J;
(a) Stress vs. strain on front and rear strain gauges and
(b) Specimen after compression failure; damage area after impact is shown in blue and damage during compression is shown in green.

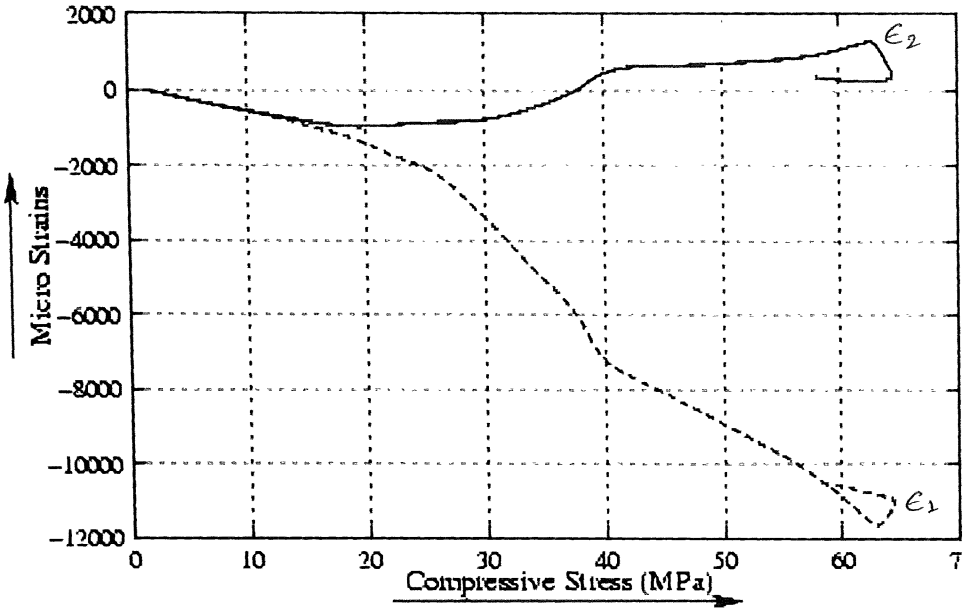

(a)

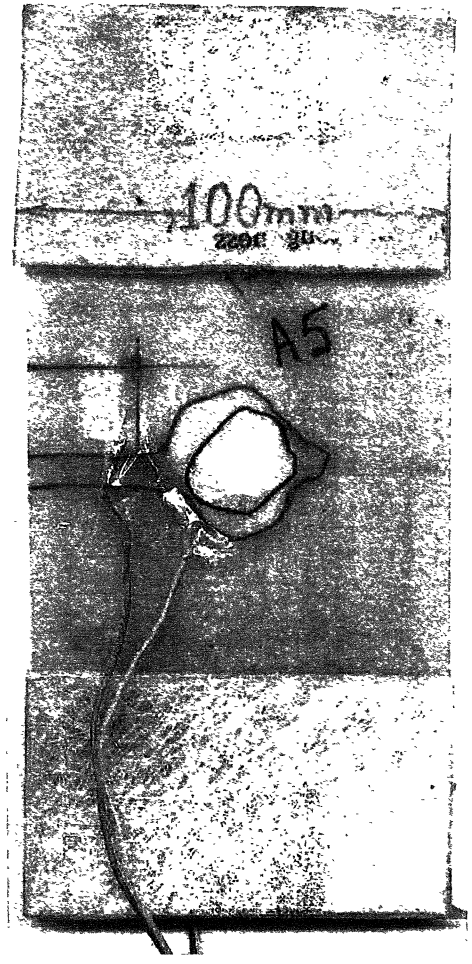

(b)

Fig. 4.15 GAL specimen (A 5), with impact energy of 11.84 J;
(a) Stress vs. strain on front and rear strain gauges and
(b) Specimen after compression failure; damage area after impact is shown in blue and damage during compression is shown in green.

Chapter 5

Conclusions and Suggestions for Future Work

5.1 Conclusions

The experimental setup is developed to perform the impact test and the compression test on panels for determination of compressive strength of the FRP panels after impact. An air gun setup is used to perform the impact test on the panels. Compressed air is used to accelerate the striker in the gun barrel; a solenoid valve is used to release the compressed air stored in the gas chamber. A laser torch mounted at the mouth of the gun barrel is used to evaluate the velocity of the striker bar with the help of the oscilloscope. The impacted panels were prepared for compression test. An anti-buckling guides are used to suppress the buckling of the specimen during compression.

CAI test was performed on two types of composite laminates. It was found that the compressive strength of impacted GFL specimens is more than three times of the compressive strength of impacted GAL specimens. Thus the GFL specimens are better in CAI tests than the GAL specimens.

To make a large FRP structure, T-joints are extensively used. It is therefore important to charactrize the impact behaviour of T-joints. A specially designed T-pull specimen is employed for determining impact behaviour. A fixture for performing tension test after impact on T-pull specimen is designed,

fabricated and make functional. The T-pull specimens were supplied by NAL Bangalore. The developed T-pull test fixture is used to perform a test on the T-pull specimen; the preliminry results show that the developed experimental setup works well.

5.2 Future Scope

- Impact energy should be varied to determine the CAI strength.
- Compression after impact test can also perform on different configurations of angleply laminates.
- In order to see the effect on compressive strength after impact by runway debris, ceramic impactor can be used.

References

Chaturvedi, S.K. and Sierakowski, R.L. (1983) "Impact loading in filamentary structural composites," *Shock and Vibration Digest*, vol. 15, pp. 13–31.

Joshi, S.P. and Sun, C.T. (1985) "Impact induced fracture in a lmainated composite," *J. Composite Materials*, vol. 19, pp. 51–66.

Malvern, L.E., Sierakowski, R.L. and Takeda, N. (1982) "Microscopic observation of cross-section of impacted composite laminate," *Composite Technology Review*, vol. 4, pp. 40–44.

Ross, A.C., Sierakowski, R.L. and Takeda, N. (1982) "Delamination-crack propagation in ballastically impacted glass/epoxy composite laminates," *Experimental Mech.*, vol. 22, pp. 20–25.

Cantwell, W.J. and Morton, J. (1985), "Detection of impact damage in CFRP laminates," *Composite Structures*, vol. 3, pp. 241–258.

Abbott, R., Jonas, P.J. and Kassapoglou, C. (1988) "Compressive strength of composite sandwich panels after impact damage. An experimental and analytical study," *J. Composite Technology and Research*, vol. 10, pp. 65–73.

Gawahale, A.R. (1990) "Fracture tooughness behaviour of FRPs reinforced by aluminium particles at te interfaces," M.Tech. Thesis. I.I.T., Kanpur.

Liu, D. (1990) "Delamination resistance in stitched and unstitched composite plates subjected to impact loading," *J. Reinforced plactic and Composites*, vol. 9, pp. 59–69.

Meester, P., Verposest, I. and wevers, M. (1989) "2.5 D–Fabrics for delamination Resistant composite laminates," *ICCM VII*, Guanzhou, China, vol. 2, pp. 322–328.

Sun, C.T. and Rechak, S. (1988) "Effect of adhesive layers on impact damage in composite laminates," *Testing and Design (Eighth Conference)*. ASTM STP 972. J.D. whitcomb, ed., American Society for Testing and Materials, Philadelphia, pp. 97–123.

Gillespie, J.W., Maikuma, H. and Whitney, J.M. (1989) "Analysis and experimental characterization of centre notch flexural test specimen for mode-II interlaminar fracture," *J. Composite Materilas*, vol. 23, pp. 756–786.

Clark, G. (1989) "Modelling of impact damage in composite laminates," *composites*, vol. 20, pp. 81–94.

Stellbrink, K. (1983) "On the behaviour of impact damaged CFRP laminates," *Fibre Science and Technology*, vol. 18, pp. 81–94.

Agrawal, B.D. and Broutman, L.J. (1990) "*Analysis and Performance of Fiber Composites,*" Second Edition, John Wiley and Sons Inc.

Kumar, P. and Rai, B. (1990) "Reduction of impact damage in KFRP through replacement of surface plies with glass fabric plies," *Journal of Composite Materials*, Technomic Publishing Co., Inc. Pennsylvania. vol. 25, pp. 694–702.

Asp, L.E., Nilsson, S. and Singh, S. (2000) "An experimental investigation of the influence of delamination growth on the residual strength of impacted laminates," *Composites Part A*, Elsevier Science Publisher Ltd., England. vol. 32, pp. 1229–1235.

Besant, T., Davies, G.A.O. and Hitchings, D. (2001) "Finite element modelling of low velocity impact of composite sandwich panels," *Composite Part A*, Elsevier Science Publisher Ltd., England. vol. 32, pp. 1189–1196.

Borst, R.D. and Remmers, J.J.C. (2001) "Delamination buckling of fibre-metal laminates," *Composites Science and Technology*, Elsevier Science Publisher Ltd., England. vol. 61, pp. 2207–2213.

Cheon, J.S., Im, Y.T. and Lee, S.M. (1999) "Experimental and numerical study of the impact behavior of SMC plates," *Composite Structures*, Elsevier Science Publisher Ltd., England. vol. 47, pp. 551–561.

Curtis, P.T., Hawyes, V.J. and Soutis, C. (2001) "Effect of impact damage on the compressive response of composite laminates," *Composites Part A*, Elsevier Science Publisher Ltd., England. vol. 32, pp. 1263–1270.

Green, E.R., Morrison, C.J. and Luo R.K. (2001) "An approach to evaluate the impact damage initiation and propagation in composite plates," *Composite Part B*, Elsevier Science Publisher Ltd., England. vol. 32, pp. 513–520.

Guild, F.J., Pavier, M.J. and Short, G.J. (2001) "The effect of delamination geometry on the compressive failure of composite laminates," *Composites Science and Technology*, Elsevier Science Publisher Ltd., England. vol. 61, pp. 2075–2086.

Herszberg, I., Khondker, O.A. and Leong, K.H. (2001) "Study of composite compressive properties du to biaxial deformation of the weft-knitted glass fabrics," *Composite Part A*, Elsevier Science Publisher Ltd., England. vol. 32, 1303–1309.

Hou, J.P., Petrinic, N. and Ruiz, C. (2001) "A delamination criterion for laminated composites under low-velocity impact," *Composites Science and Technology*, Elsevier Science Publisher Ltd., England. vol. 61, pp. 2069–2074.

Johnson, A.F., Pickett, A.K. and Rozycki, P. (2001) "Computational methods for predicting impact damage in composite structures," *Composites Science and Technology*, Elsevier Science Publisher Ltd., England. vol. 61 2183–2192.

Naik, N.K. and Meduri, S. (2001) "Polymer-matrix composites subjected

to low-velocity impact: effect of laminate configuration," *Composites Science and Technology*, Elsevier Science Publisher Ltd., England. vol. 61, pp. 1429–1436.

Olsson, R. (2000) "Mass criterion for wave controlled impact response of composite plates," *Composites Part A*, Elsevier Science Publisher Ltd., England. vol. 31, pp. 879–887.

Abrate , S. (1998) "*Impact on Composite Structures,*" First Edition, Cambridge University Press.

Zhou, G. (1998) "The use of experimentally-determined impact force as a damage measure in impact damage resistance and tolerance of composite structures," *Composite Structures*, Elsevier Science Publisher Ltd., England. vol. 42, pp. 375–382.